CVD grown single crystal diamond: a review

Jean-Charles Arnault, Samuel Saada, V. Ralchenko

CVD grown single crystal diamond: a review

J.C. Arnault[1*], S. Saada[2], V. Ralchenko[3, 4]

[1] *Université Paris-Saclay, CEA, CNRS, NIMBE, 91 191 Gif sur Yvette Cedex, France*
[2] *CEA, LIST, DM2I, F-91191 Gif-sur-Yvette, France*
[3] *Prokhorov General Physics Institute of Russian Academy of Sciences, Vavilov str. 38, Moscow 119991, Russia*
[4] *Harbin Institute of Technology, Harbin 150080, P.R. China*

* jean-charles.arnault@cea.fr

Abstract

With its outstanding physical properties, single crystal diamond is the material of choice for future power electronics and quantum devices. The later application field is based on the optical and spin properties of color centers hosted in diamond lattice. Two synthesis methods are currently developed to grow high quality diamond: high pressure and high temperature (HPHT) synthesis and chemical vapor deposition (CVD). This review describes the state of the art of single crystal diamond growth by CVD, either starting with diamond substrate (homoepitaxy) or controlling diamond epitaxial nucleation on a foreign substrate (heteroepitaxy). Progress on substrates, dislocation propagation and reduction of structural defects, doping, upscaling and applications are reviewed. In light of recent progress, future challenges and the respective roles of homoepitaxial and heteroepitaxial materials in the applications roadmap are discussed.

Keywords: Single crystal diamond, Homoepitaxy, Heteroepitaxy, State of the art, Applications

1. Introduction

Single crystal diamond is the ultimate material for high voltage, high temperature and high frequency applications. Its electrical and thermal properties outperform those of other wide band gap semiconductors like 4H-SiC, GaN or Ga_2O_3.[1] Its high mobility for electrons and holes and its excellent resistance to radiation are also highly valuable for detectors in nuclear and high-energy physics experiments.[2] In addition to its outstanding electronic and thermal properties, diamond can host a wide range of color centers involving impurities and vacancies (NV, SiV, GeV,…) that possess interesting optical and spin characteristics.[3] This explains the fast development of quantum applications based on diamond materials (films, nanoparticles) within the last years. Indeed, such systems are very promising for quantum photonics and plasmonics[4], quantum computer[5], magnetometry[6], temperature sensing[7] or hyperpolarization.[8]

For these application fields, diamond films of excellent crystalline quality are required. Moreover, power devices need an accurate control of the diamond doping. While p-type boron doped diamond is nowadays optimized, n-type phosphorous-doped diamond is still challenging. For quantum applications, the current developments aim for a fine tuning of impurities (nitrogen, silicon, germanium,…) incorporated into diamond lattice, either during chemical vapor deposition (CVD)[9], high pressure high temperature (HPHT)[10] synthesis or by alternative methods like ion implantation.[11] The objective is to finely control the concentrations of color centers as well as their accurate location into diamond (spatial and depth). In addition, technological pathways for growth of large-scale single crystal diamond are essential to facilitate the developments of electronic and quantum applications.[12]

The present report aims to provide an update on the advances in single crystal diamond grown by CVD. For the state of the art of HPHT synthesis, one can refer to the following review.[13] Two strategies are currently investigated to grow high quality diamond by CVD: the first one starts from a diamond substrate (homoepitaxy) while the second uses substrates of different natures (heteroepitaxy). For both cases, progress on substrates, growth mechanisms and reduction of structural defects, doping, upscaling and applications are reviewed. More specific issues like nucleation for the heteroepitaxy pathway or fast CVD growth conditions for homoepitaxial diamond are also considered. In light of the latest advances, conclusions on future challenges are then drawn and the respective roles of homoepitaxial and heteroepitaxial materials in the applications roadmap are discussed.

2. State of the art

2.1 Homoepitaxy

Homoepitaxial diamond films are deposited on high quality polished single crystal diamond plates (substrates) in CVD reactors with different approaches to gas activation.[14,15] Below we consider the aspects of CVD diamond synthesis based on microwave plasma assisted chemical vapor deposition (MPCVD) only as it is this type of plasma which provides very high film purity matched to high growth rates over large area. Ultrapure electronic grade CVD diamond with nitrogen concentration <5 ppb is currently commercially available from *Element Six*. Particularly, the material of this sort demonstrated record high electron mobility, a factor of two better than for the best natural type IIa diamond crystals,[16] that is crucial for electronic applications. The CVD diamond shows thermal conductivity of ≈24 W $cm^{-1}K^{-1}$ at room temperature, the highest value ever measured for synthetic diamonds with natural isotopic composition, and an order of magnitude higher, of 278 W $cm^{-1}K^{-1}$ at lower temperatures (63 K).[17] The search for methods to reduce defect density, enhance growth rate and provide prolonged non-stop growth, develop precisely controlled doping procedures, to obtain the material tailored for particular applications is one of the major directions in CVD diamond research. Homoepitaxial diamond films are grown on HPHT and CVD diamond single crystal substrates. The CVD growth in almost all cases is performed on (100)-oriented substrates as the {100} crystal face yields the lowest density of structural defects in the produced epilayers. Nevertheless, reports on high quality CVD SCD (Single Crystal Diamond) growth on substrates with different orientations, such as (111)[18,19] or (113)[20,21] are available.

2.1.1. Substrate preparation for homoepitaxy

A pretreatment to remove defects on the substrate surface is needed as they may induce further defects, such as threading dislocations, in the growing epitaxial layers. Polishing of the substrates results in formation of subsurface damage layer the thickness of which is of the order of a few micrometers in case of mechanical polishing with "scafe".[22] Yurov et al.[23] observed an enhanced etching rate in hydrogen microwave plasma of the first surface layer for both IIa type HPHT and CVD (100)-oriented substrates compared to the bulk diamond etching. They assigned such kinetics to the presence of the polishing-induced damaged layer, and estimated its thickness of ~1 μm for a CVD substrate and ~0.2 μm for the HPHT substrate. The widespread substrate pretreatment to remove surface damage includes H_2/O_2 microwave plasma etching of the substrate before growth.[24] However, the H_2/O_2 plasma etching is strongly anisotropic and leads to the appearance of deep etch pits and high surface roughness. Achard et al. [25] combined H_2/O_2 plasma etching as a 1st step with smoother surface treatment such as reactive ion etching-inductively coupled plasma (RIE-ICP) etching or Chemo-Mechanical Polishing (2nd step) and they showed a significant reduction in dislocation density of the thick CVD epitaxial layers: similar defect density as in the initial HPHT substrate was obtained. Smooth, homogeneously etched SCD surfaces were obtained with ICP treatment using an argon–chlorine mixture.[26,27] Such gentle etching did not increase surface roughness of the HPHT diamond (at least up to the 6-μm etching depth). The CVD crystal grown on an HPHT substrate pretreated with ICP revealed a dramatic reduction in the dislocation density.[26] Also $Ar/O_2/CF_4$ RIE plasma treatment of the substrates was employed to remove sub-surface polishing damage to the depth up to 10 μm.[28]

2.1.2. High rate growth

The search for growth regimes which combine high quality of SCD with high growth rate is one of main priorities of CVD technology, especially in case of thick crystal production. The CVD diamond

synthesis is sensitive to many process parameters, such as gas pressure in the reactor,[29,30] methane concentration,[31] substrate temperature,[29,32] absorbed microwave power density,[29,32] nitrogen contamination,[29,33] substrate holder geometry,[34] and others. By combining several beneficial parameters in one recipe Liang et al.[35] reported SCD growth up to 18 mm in thickness at gas pressures of up to 350 Torr. Growth rates of up to 165 μm/h at 300 Torr at high power density have been achieved with N_2 addition in gas. They speculated that "next generation MPCVD reactors should be capable of generating stable plasma at chamber pressures above 1 atm, resulting in growth rate increased to 1 mm/h under such conditions". This prediction still is not realized in experiment.

Optimization of the reactor itself and deposition process is not an easy task because of complexity of the processes involved. To reveal the isolated effect of one variable parameter, normally many SCD samples with thickness of at least a few hundreds of microns should be produced, which is a long procedure. Bushuev et al.[32,36] dramatically reduced the time needed and suggested an express method to perform experiments with one or several variable parameters in one run, on a single substrate, without switching off the plasma. They used a low-coherence interferometric *in situ* control of the growth rate and sample thickness ~~in any moment~~. For example, substrate temperature T_s was changed in steps and the growth rate was measured at each step after the process had equilibrated. Typically, 5 to 10 min of the linear growth time was enough to determine the growth rate at fixed *T*s with high accuracy (see **Figure 1**). The kinetics data thus determined, particularly, activation energy, are valuable to the growth modeling.

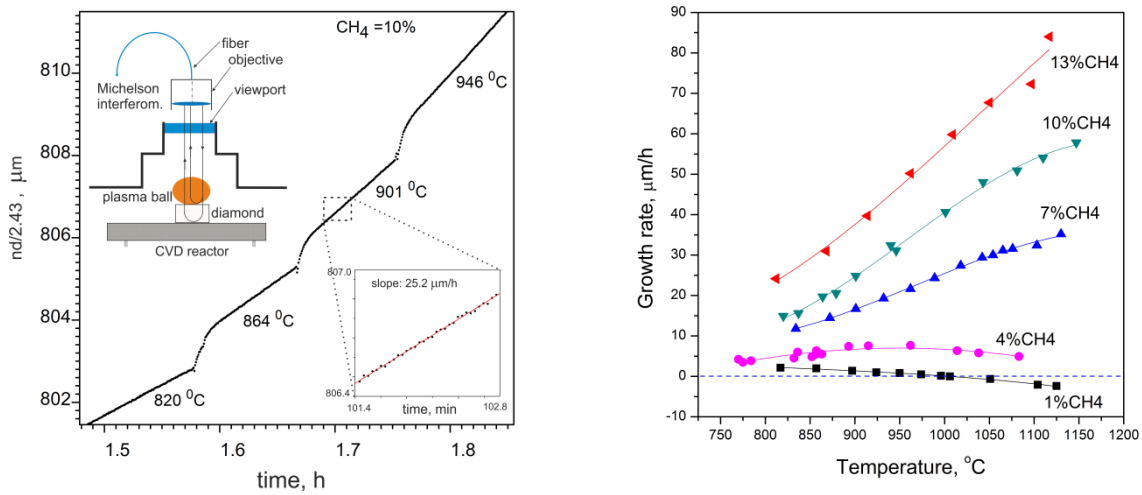

Figure 1. *Left panel*: Evolution of epilayer thickness with time under consecutive rise in steps of substrate temperature T_s at 10% CH_4 content as measured with low-coherent inteferometer. The temperature is indicated for each segment. The linear segments correspond to the growth with constant rate. The transitions between two segments are due to temperature dependence of diamond refraction index and sample thickness product $n(T)d(T)$. *Inset*: optical scheme of LCI measurements of sample thickness. *Right panel*: Dependence of growth rate on substrate temperature at different CH_4 contents in gas mixture. Note the net etching for 1% CH_4 at T_s >1000°C.[32] Reproduced with permission. Copyright 2017, Elsevier.

2.1.3. Growth on multiple substrates

For up-scaling the industrial production of SCD MPCVD reactors operated at 915 MHz frequency have been introduced, which maintain a larger size plasma compared with 2.45 GHz CVD systems,.[37] With a 75 kW 915 MHz reactor high production rates of up to 300 diamond single crystals placed on a 300 mm diameter substrate holder was reported by Liang et al.[38] They demonstrated production rates of up to 100 g/day of SC diamonds, with 25% of the material categorized as colorless. To achieve better plasma uniformity one has, however, to decrease the pressure down to 100-130 Torr, with a cost of a reduction in growth rate.

2.1.4. Growth of large size plates

Since many applications need wafer size SC diamond, ~~methods to increase the CVD plates number having in disposal seeds of limited dimensions only,~~ methods to increase the grown plates area were explored. By growing a thick CVD layer it is possible to enlarge the initial area of the substrate by a factor of two since growth also occurs laterally from the substrate.[39] Nad et al.[40] grew single crystals in an optimized pocket substrate holder, and reported the lateral SCD surface area increased between 1.7 and 2 times greater than the initial seed surface area during one continuous run. Using the side faces as growth surfaces a half-inch single-crystal CVD diamond seed crystal was synthesized and half-inch freestanding single-crystal CVD diamond plates were produced from the seed obtained by lift-off technique.[41] A more promising way to extend the SCD size to inch-scale is known as "mosaic" growth.[42,43] It uses the overgrowth of homoepitaxial diamond on identically oriented seeds synthesized diamond substrates assembled in one mosaic-tiled geometry, with following separation of the formed monolith from the substrate.[44,45] Mosaic wafers as large as 40 × 60 mm^2 produced on arrays of 10 × 10 mm^2 "clone" substrates were demonstrated.[45] Dielectric properties of the mosaics with areas up to 8 cm^2 and thickness of ~ 1 mm were measured in 90–170 GHz frequency range, and loss tangent *tanδ* of less than 2 × 10^{-5} has been determined.[46] This value is as low as that of the high quality polycrystalline diamond developed for many years as components of high power gyrotrons.[47]

While the major volume of the mosaics can be a high quality low-stress material, the coalescence boundaries (junctions) between the blocks contain an enhanced defect concentration and stress[48-50] according to analysis with Raman spectroscopy. The stressed zone may extend to distances of the order of 100 μm from the junction (**Figure 2**). The defects, such as bundles of threading dislocations (TD) in the junction region (the dislocation density in the TD bundle region was <10^{10} cm^{-2}) are shown by Ohmagari et al.[49,50] to locally degrade electronic performance of devices such as Schottky barrier diodes. To further improve the device uniformity these authors introduced a buffer layer to mitigate the influence of coalescence boundaries on the diamond mosaic wafer. The buffer layer was a diamond film with tungsten impurities growth by hot-filament CVD, and the tungsten incorporation effectively suppressed dislocation propagation from the mosaic substrate to the epilayer. For high power devices the ability of diamond to effectively dissipate generated heat is critically important, and one may expect that the defects localized around the junctions can degrade also the *in-plane* thermal conductivity, by forming thermal barriers. This issue is worth of further experimental verification.

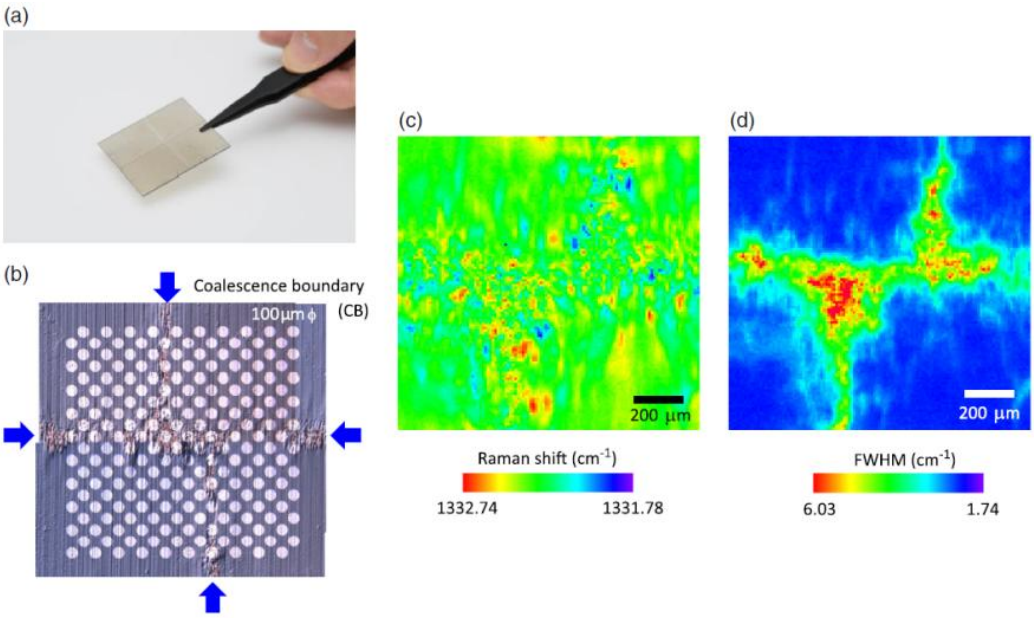

Figure 2. a) Photograph of a diamond mosaic wafers (40mm × 40 mm) in which pieces of free standing plates are connected laterally by CVD growth. b) Optical microscopic image of Schottky barrier contacts fabricated near junctions. The electrode diameter was 100 μm. Confocal Raman imaging near the junctions showing c) Raman shift and d) full width at half-maximum (FWHM) mapping.[50] Reproduced with permission. Copyright 2019, Wiley-VCH GmbH.

2.1.5. Doping

Diamond is wide-band gap (5.45 eV) semiconductor with high breakdown field of 13 MV/cm and high intrinsic carrier mobilities, of up to 3800 cm V^{-1} s^{-1} and 4500 cm V^{-1} s^{-1} for holes and electrons at room temperature, respectively,[16] very promising for next generation of high power electronics, such as diodes and microwave transistors.[51,52] Doping is needed to provide *p*-type or *n*-type conductivity for designed device structures. Boron in diamond gives *p*-type conductivity with activation energy E_a = 0.37 eV, while phosphorus gives *n*-type conductivity with E_a = 0.59 eV. The doping is performed by adding the respective precursor, most often diborane B_2H_6[53] or phosphine PH_3[54] in the process gas. Since in B-doped diamond hole mobility decreases significantly with dopant concentration, delta doping has been attempted to mitigate this effect at enhanced dopant concentrations by forming a very thin (of the order of 1 nanometer), highly boron-doped ([B] ≥ 10^{20} cm^{-3}) layer inside intrinsic diamond.[55,56]Butler et al.[56,57] reported hole mobility of up to 120 cm^2 V^{-1} s^{-1} in a 1 nm thick delta layer with estimated boron density of ≈4×10^{20} cm^{-3}. Their CVD reactor with fast exchange of feed gas was also used to form delta-doping with nitrogen to create a 2D ensemble of nitrogen-vacancy color centers with well defined positions, which is important for optical quantum technologies.[58,59] "Surface transfer doping", an alternative approach to form a *p*-type layer, exploits hydrogen surface termination, which combined with adsorbates, induces a quasi-2D hole channel a few nanometers below the surface.[52,60] Field-effect transistors (FET) on H-terminated diamond were realized by a number of groups[61-64] with cutoff frequency above 50 GHz.[65] The H-terminated surface is easily prepared by exposure of the diamond substrate to hydrogen plasma, which results in sheet carrier densities of the order of 10^{13} cm^{-2}. Further deposition of a protective metal oxide thin film is used to stabilize the diamond's surface conductance.

A great increase in engineering of color centers in diamond for photonic and quantum technologies has been reported in the last decade. The optically active defects with bright luminescence in the visible and near infrared spectral range, such as impurities related to vacancy in the diamond lattice: nitrogen-vacancy (NV), silicon-vacancy (SiV), germanium-vacancy (GeV), and more recently PbV and SnV centers, are considered as candidates for single photon emitters for realisation of solid-state quantum photonics.[4,66] These centers are stable at room temperature and promise to create quantum bits operating in ambient conditions. While the color centers can be formed in diamond by ion implantation,[67] *in situ* doping during diamond growth is preferrable ~~to the aim~~ to avoid remnants of the implantation induced-damage that could left even after high temperature annealing. Representative examples are doping with gaseous silane SiH_4[68] and germane GeH_4[69] precursors added to the plasma, the concentration of the respective color center being controlled by the dopant flow rate. It was discovered[70] that the dephasing time T_2 of single electron spins of NV center in ultrapure diamond enriched with ^{12}C isotope strongly increases up to 1.8 ms. Deposition of thin diamond films on (100) substrates using isotopically purified methane is a convenient method to improve the spin properties.[71]

2.1.6 Applications of homoepitaxial films

Production of thick, of a few millimeters and more, diamond crystals of high quality remains one of important research activities, primarily for jewelry. Another need for thick bulk crystals is stimulated by interest in preparing low-dislocation substrates for epitaxy. As dislocation in the CVD layer propagates from the substrate/film interface mostly parallel to the growth direction, the produced bulk (100)-oriented CVD crystal can be sliced vertically (in parallel to the growth direction) to fabricate a batch of new substrates in such a way, that the side [100] plane is almost free from dislocations which cross the [100] face.[72] The further growth on the side plane confirmed a strong decrease by an order of magnitude in dislocation density.[26,72]

The SC CVD diamond is used in X-ray beam position monitors,[73] X-ray monochromators[74] and splitters,[75] detectors of charged high energy particles,[76,77]neutrons,[78-80] UV light,[81] and in dosimeters in radiotherapy, particularly for proton therapy[82] to combine good electronic properties and radiation hardness. Diamond detector structure with pair of planar metal electrodes on two sides of the diamond plate is a common feature of such devices (UV sensors may have electrodes on one plane only). The charge carriers created by ionizing radiation are collected on the electrodes, so there is no reason to make the detector thickness exceed the charge collection distance *L* (typically *L* <500 μm). This limits the volume of the detector and potential amount of charges to be registered. Recently, the idea of 3D structures for the electrodes has received an interest. Oh et al.[83] proposed a novel diamond detector with buried graphitic vertical electrodes on a single crystal for ionizing radiation monitoring.

Vertical conductive graphitic micro-pillars with 200 μm interdistance were fabricated in bulk via laser-induced local graphitization of diamond by moving the tightly focused laser beam (3 ns pulses were used). Rows of the buried graphite pillars were connected by deposited metallic contacts. With fixed interdistance between the electrodes the applied voltage does not depend on the film thickness. The following investigation[84] was dedicated to the realization of a larger 3D prototype (with the graphitic wires formed by 100 fs pulses at 800 nm wavelength) to be tested as position sensitive detector and particle tracker under 120 GeV proton beam irradiation. The sensor operated at much lower applied voltage compared to the planar version of the device of the same crystal, demonstrating the advantages of a 3D diamond detector. To overcome the necessity of metallization and photolithography processes, Lagomarsino *et al*.[85] and Kononenko *et al*.[86] demonstrated all-carbon detectors with surface graphitic stripes (produced also by the laser) for connections of the pillars along parallel paths. Recently, an all-carbon transmissive X-ray imaging pixel detector was demonstrated which is capable of imaging a synchrotron X-ray beam profile with the resolution as high as 600 nm.[87] As the detector includes no metallization in the beam path it introduces fewer absorption edges that may interfere with beamline experiments. It is important that the graphitic wires extend deep into the crystal (for a few millimeters[88]) in order to guarantee that a large volume fraction of the diamond contributes to the sensing signal. The material modified by laser-treatment is in fact a mixture of the diamond and graphite phases; its nature is strongly dependent on process parameters as wavelength of light, pulse duration and repetition rate, size of the focused laser spot, fluence and velocity of the focal plane through the diamond.[89,90].The space in proximity to the graphitic pillars is enriched with defects and stress[91] which might reduce the detector performance. Nevertheless, a high charge collection efficiency of 96% was obtained under MeV electrons irradiation. A recent study[92] showed the structure of the laser-induced graphitic pillars to be more complex than it was assumed earlier. In particular, the graphitic channel looks tree-like with graphitized cracks fanning out from the central root. This observation can explain the high (compared to that known for graphite) electrical resistance of the pillars. Therefore, a careful choice of laser irradiation parameters is needed to avoid this detrimental effect. More details on fabrication and performance of 3D diamond detectors can be found in a review.[93]

Great progress was achieved in last decade in development of diamond Raman lasers (DRL)[94, 95]. This type of laser converts the input pump laser beam with frequency ω_{pump} to output radiation spectrally shifted by the frequency of optical phonon ω_{ph} of the particular crystal due to Raman effect (for diamond ω_{ph} = 1332 cm^{-1}). Generation of Stokes and anti-Stokes of 2nd and higher orders are possible, extending the range of output wavelength variation. A large fraction of the pump energy transforms to shifted energy owing to stimulated Raman scattering (SRS). Diamond is an excellent medium for Raman lasers due to a unique combination of excellent material properties : high Raman gain, large Raman shift, simple single-line Raman spectrum, wide transparency range, high thermal conductivity and low thermal expansion coefficient. The SRS effect in solids was observed for the first time by Eckhardt *et al*.[96] who studied a natural diamond crystal. The interest to DRL revived with appearance of CVD diamond samples of optical quality. SRS properties of CVD diamond were reported by Kaminskii with co-authors, first for polycrystalline diamond,[97] then for single crystals,[98] who used a single pass geometry. Soon, the first Raman laser emitting at 573 nm has been demonstrated by Mildren et al.[99] by placing the crystal inside the cavity. The DRL development was sped up due to the availability of high quality CVD crystals of large size with low optical absorption, low dislocation density, low birefringence. Because temperature gradients within diamond crystals are strongly reduced owing to extremely high thermal conductivity, the detrimental effect of thermal lensing is much weakened for diamond compared to other crystals used for Raman lasers. This allows obtaining DRL of very high powers: Antipov et al. [100] reported on 1.2 kW DRL operated at 1.24 μm with pump at 1.06 μm. Currently, DRL generation was realized between UV and mid IR spectral range, pulse length from femtoseconds to continuous wave (CW) regimes.[95,101]

2.2 Heteroepitaxy

2.2.1 Substrate for heteroepitaxy: a strategic starting point

The choice of the substrate for heteroepitaxial growth is essential because it greatly influences the crystalline quality of the diamond films obtained after growth. The criteria for substrate selection are numerous and include not only the crystal structure, the lattice constant, the thermal expansion

coefficient, but also the substrate stability under CVD plasma environment and the surface reactivity which is a critical point to get diamond nucleation.

A large variety of materials have been tested and used for diamond heteroepitaxy: Si[102], SiC[103], TiC[104], Co[105], Pt[106], Ir[107], c-BN[108], Al_2O_3[109], Ni[110] and Re[111]. The formation of a continuous film requires the presence of a sufficiently high density of nuclei and the quality of the film is intimately linked to the disorientation of the nuclei. The crystalline quality of heteroepitaxial films obtained on iridium is an order of magnitude better than other substrates and it is today recognized as the best material for diamond heteroepitaxy. Nucleation mechanisms more specific to iridium will be detailed in part 2.2.2.

To limit the cost of the substrates, to reduce the thermal stress and move towards larger substrates, multilayer substrates have been developed with iridium buffer layers deposited on metal-oxide layers on silicon substrates ($SrTiO_3$/Si and YSZ/Si[112]), oxide substrates like MgO[113] and more recently sapphire [114] and $KTaO_3$[115]. The optimization of the iridium layer is very dependent on the nature of the substrate and the deposition process [116, 117]. While the growth of (100) oriented diamond films is in the majority, (111) orientation is also being studied, using 3C-SiC/Si (111) [118] and recently Ru/c-sapphire substrates. [119]

2.2.2 Diamond nuclei and nucleation mechanisms on iridium

To grow heteroepitaxial diamond films, an accurate control of diamond nucleation is required with *nuclei* in epitaxial relationship with the substrate. Among the investigated nucleation techniques[120], Bias Enhanced Nucleation (BEN), first reported by Yugo et al.[121], has been established as the most powerful process to generate epitaxial diamond *nuclei* on different heterosubstrates (Si, 3C-SiC, Ir,…). It consists of negatively polarizing the substrate with respect to the reactor walls or a counter electrode, immerged in a plasma generated by microwaves or a DC discharge.[122] This produces an ion bombardment of the substrate by positive ion species. As shown previously (part 2.2.1), most of the current works focus on the iridium surface due to its specific reactivity with carbon that includes solubility, segregation and subplantation mechanisms.[123] Let us note that some research activities continue on cubic silicon carbide.[124] On iridium, during BEN, diamond nucleation mainly competes with surface roughening and with the formation of an amorphous carbon overlayer. Diamond *nuclei* that are generated during BEN in domains close to 2D patterns, exhibit a high epitaxial rate (> 90 %). No obvious growth of *nuclei* was observed during BEN contrary to the growth in islands (Volmer Weber mode) reported for other heterosubstrates such as silicon or cubic silicon carbide.[125] Indeed, the stronger BEN conditions, typically applied to iridium, with a bias voltage up to – 400 V, can induce diamond etching. Consequently, without further growth, such *nuclei* remained invisible using high resolution transmission electron microscopy (HRTEM).[126] Nevertheless, their presence was detectable via X-ray photoelectron diffraction[127], Auger electron spectroscopy, X-ray absorption near edge structure, high-resolution electron energy loss spectroscopy[112] or via scanning electron microscopy (SEM) contrast difference in areas called domains.[128]

Based on their numerous investigations of BEN on iridium, Schreck et al reported on a nucleation model called Ion bombardment induced buried lateral growth (IBI-BLG).[129] It considers the effects of ion bombardment occurring during BEN within the hydrogenated amorphous carbon layer formed at the iridium surface **(Figure 3)**. According to simulations, an equilibrium is established between the implantation of positive ions and a chemical etching. Under such conditions, diamond nucleation can occur at the iridium surface. *Nuclei*, protected by the amorphous carbon layer, then undergo lateral growth in a pseudo-2D mode (Figure 1c). After BEN, the hydrogenated amorphous carbon layer is etched away under MPCVD plasma and the growth of epitaxial diamond nuclei can take place.

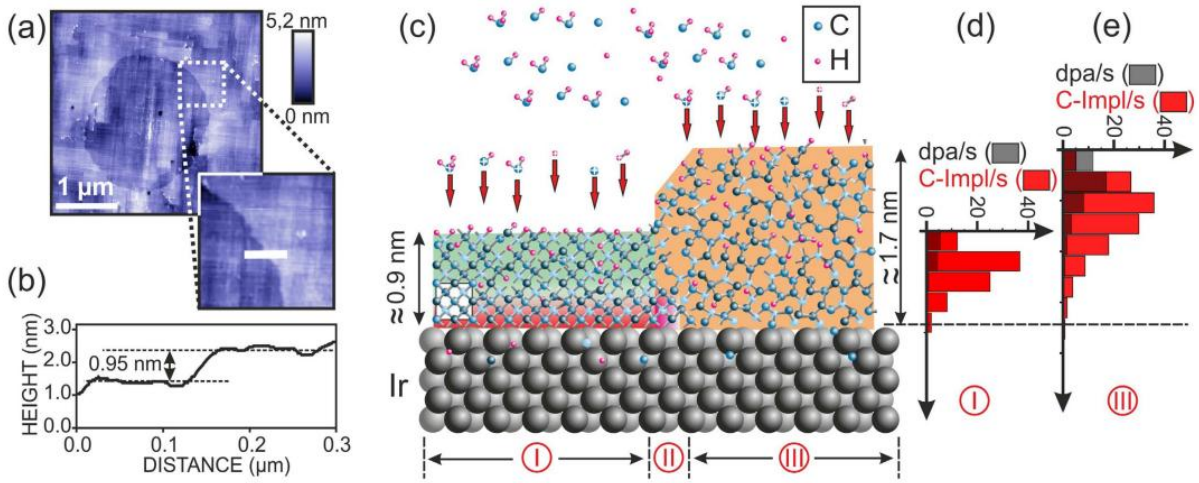

Figure 3. Scheme of the ion bombardment induced buried lateral growth (IBI-BLG) model, (a) AFM picture at a domain border; (b) height profile indicated on (a); (c) scheme of the layer structure; (d) and (e) simulation of depth profiles of implanted carbon species. Reproduced with permission. [129] Copyright 2017, Nature.

2.2.3 Growth mechanisms

During the coalescence of highly dense diamond *nuclei* (typically $10^{11}/cm^2$), dislocations are created mainly due to the large mismatch between diamond and iridium lattices (7%) to accommodate strain. In the first stages of textured growth on iridium, the polar and azimuthal mosaicities, tilt and twist, respectively, decreases with the film thickness.[130] Indeed, a combination of experiments and simulations demonstrated that two neighboring islands could merge via a disclination mechanism. This is likely due to the weak misorientation between epitaxial islands on iridium, typically lower than 1°, compared to several degrees on silicon or cubic silicon carbide. Consequently, the density of dislocations drops with the growth of heteroepitaxial films of several microns. Due to the strong increase of the Raman scattering, Ultra Violet Raman, operating at 325 nm, is well adapted to characterize the crystalline quality and the strain within such thin heteroepitaxial films.[131] The dislocation density within the diamond lattice can be estimated either from HRTEM images[132], Cathodoluminescence (CL), as dislocations act as non-radiative recombination centers for electron-hole pairs and excitons, [133] or from the counting of etch pits generated by H_2/O_2 plasma at the film surface.[134] According to HRTEM, pure edge dislocations are more efficiently reduced. The analysis allows prediction of the evolution of the dislocation density proportional to the inverse of the film thickness.[135]

Several HRTEM studies were then performed to better understand the propagation of dislocations during the growth of heteroepitaxial films on iridium. The main objective was to identify the parameters affecting their propagation that is highly dependent on the macrostructure of the diamond growth surface (terraces, risers) as shown on different off-axis substrates.[136] Dislocation bending is also promoted by nitrogen addition in the gas phase that induces step bunching at the diamond growth surface. Tilting angles higher than 20° towards the step flow direction were measured for all kinds of dislocations on cross-section images in the riser growth area **(Figure 4).**[132] This strengthens interactions between dislocations that favor their annihilation. In the absence of nitrogen in the gas phase, the induced bending is dependent on dislocation type.

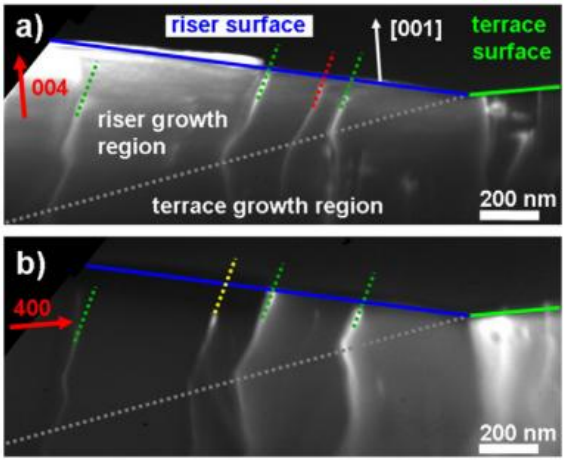

Figure 4. Cross-section TEM images taken along the [010] direction. As shown by weak beam dark field mode using 004 (a) and 400 (b) reflections, all kinds of dislocations underwent a bending with an angle higher than 20° in the riser growth region. More details are provided in the following reference. [132] Reproduced with permission. Copyright 2016, Elsevier.

Finally, the correlation between stress states and the dislocation propagation was investigated by HRTEM for diamond (111) heteroepitaxial films grown on off-axis and on-axis substrates. [137, 138]

2.2.4 Strategies to reduce dislocation density and improve crystalline quality

Performances of diamond electronic devices or radiation/particle detectors are strongly affected by structural defects. One of the current challenges is to decrease the dislocation density in high crystal quality diamond films. The dislocation density of heteroepitaxial diamond films is between 10^8 - 10^9 cm^{-2} for film of few hundreds of microns and therefore much higher than that of homoepitaxial films (between 10^2 – 10^5 cm^{-2}). The evolution of the dislocation density from early stages to thick films was described in the previous part. Thus, several strategies have been developed to reduce more drastically the density of dislocations.

The patterning of diamond nucleation to promote Epitaxial Lateral Overgrowth (ELO) is a promising approach proposed by Ando et al.[139]. The geometry of the patterns, their size and orientation are critical parameters. In the case of a stripe pattern, the orientation of the stripes influences the propagation of dislocations as the film thickens [140, 141]. Pattern nucleation region width is also a key parameter but not easy to implement at large scale because it requires the integration of nanopatterning technologies. The spacing between the stripes favors lateral growth but beyond a certain size, the nucleation of non-epitaxial crystallite on the non-cover area is detrimental. This problem has been solved by proposing a cross-band structure and leads to a dislocation density of 9 x$10^6$$cm^{-2}$ in the areas between the bands spaced at 100 µm[142]. Patterning after a growth step via a metal pattern is also a way to reduce the dislocation density as reported by Tang et al.[143]. Another concept developed by Aida et al. is based on patterning a thin diamond film followed by a growth stage to fabricate diamond micro-needles with high aspect ratio in order to produce a free standing heteroepitaxial film after a subsequent growth[144, 145, 146]. This concept therefore both reduces dislocation density, allows a nearly stress-free state to be reached and greatly facilitates film detachment by delamination. The microneedle pitch also has an influence on the diamond film quality: with a pitch of 50µm, the FWHM of the X-ray rocking curve for diamond (004) is 0.17°.

As shown in the part 2.2.3, another approach is the use of an off-axis substrate coupled with the addition of nitrogen in the gas phase that increases the probability of dislocation interactions and thus reduces the dislocation density[136]. Ohmagari et al. have recently applied a method which consist of introducing a diamond buffer layer containing tungsten metal impurities in order to create interactions with dislocations to modify their propagation; this method has been applied to heteroepitaxial films and the qualitative results obtained are promising[50].

2.2.5 Impurities incorporation in heteroepitaxial diamond

Heteroepitaxial diamond is a material of choice for electronic applications due to its high crystalline quality and its large scale (paragraph 2.2.6). The doping with boron and phosphorous atoms is then essential, to provide p-type and n-type doping, respectively. The fabrication of diodes (pin[147], Schottky[148]) allow the estimation of the crystalline quality of heteroepitaxial films.

The first reported study of boron doping was performed during diamond (001) heteroepitaxy on an iridium substrate. The boron incorporation within the diamond lattice was tuned from 10^{19} to $5x10^{20}$ boron atoms per cm^3 according to CL, secondary ion mass spectrometry (SIMS) and X-ray diffraction measurements.[149] The boron insertion enhances the biaxial stress while the role of dislocations in the stress state was confirmed (paragraph 2.2.3). HRTEM investigations revealed a segregation of boron atoms around dislocations **(Figure 5)** that is driven by the tensile strain field.[150]

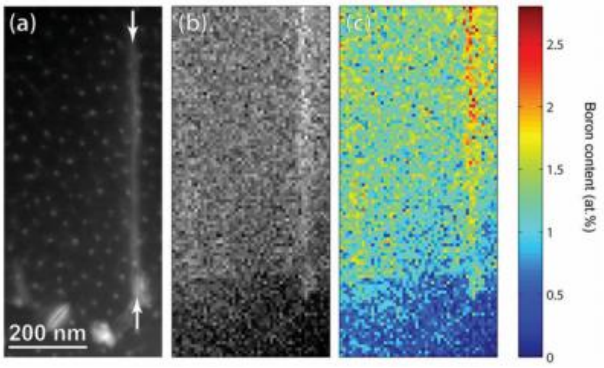

Figure 5. (a) Annular dark field Scanning TEM (STEM) image of a dislocation; (b) boron K-edge mapping; (c) boron content mapping. Reproduced with permission.[150] Copyright 2016, The Royal Society of Chemistry.

Two other research groups reported on boron doping of heteroepitaxial diamond films grown on iridium.[147, 148] The two overlayers involved in the diode devices were highly (p+; 1-$8x10^{20}$ boron atoms per cm^3) and low (p-; $4x10^{16}$- $1x10^{17}$ boron atoms per cm^3) doped epitaxial layers, a few microns thick. Up to now, only one study reported on phosphorous doping performed on heteroepitaxial diamond. The phosphorous incorporation in this overlayer, 1 micron thick, was $2x10^{17}$ phosphorous atoms per cm^3.[147]

Heteroepitaxial circular islands were grown onto iridium after a patterning by an inductively coupled plasma - reactive ion etching (ICP-RIE) treatment of the nucleation layer created under BEN.[151] Si incorporation in (100) oriented diamond was favored via a silicon wafer located in the MPCVD plasma. Among SiV color centers detected by confocal microscopy, some exhibited a narrow zero phonon line corresponding to single color centers. In parallel, NV centers were created within heteroepitaxial diamond films grown onto off axis 3C-SiC/Si (111) by adding nitrogen in the gas phase.[152] A preferential alignment of NV along the [111] direction was demonstrated by optically detected magnetic resonance (ODMR). Such behavior is suitable for enhancing sensitivity of temperature sensors.[153]

2.2.6 Progress in substrate up-scaling

Upscaling the iridium terminated substrate is a real challenge to address applications that require large substrates, often for reasons of compatibility with existing wafer processing equipment already in place in industry and for cost reductions. This is particularly true in the field of electronic devices. The medium-term objective will be to reach sizes of at least 2 inches to consider processes on multiple substrates at the same time. Although the size of the substrates is important, it only makes sense if the desired properties are homogeneous over the entire surface of the wafer and if the reproducibility of the deposits is high.

With regard to the availability of large-scale heterosubstrates, the introduction of multilayer substrates is a major advance because it allows one or more successive epitaxial growth steps to be carried out on silicon, MgO or sapphire wafers to obtain an epitaxial iridium layer. The size extension then depends on the commercial availability of the starting wafer (12 inch for silicon, 8 inch for sapphire, 2 inch for MgO).

If the availability of heterosubstrates is no longer a limitation, the main bottleneck is the nucleation stage. Today, the only pretreatment that allows epitaxy of diamond on iridium is the BEN step presented in part 2.2.2. This has the effect of creating a zone of space similar to a cathodic sheath above the substrate in which certain species are accelerated. The usual process parameters are not sufficient to reproduce this step in another reactor because the formation and properties of this space zone are intimately linked to the internal geometry of the reactor, the geometry of the substrate holder, the nature of the materials used, etc. Each research group has optimized its homemade system and process parameters in an attempt to enlarge the area impacted by the BEN. This task is all the more difficult as the parametric window to obtain epitaxial nucleation conditions is very narrow[154]. Yoshikawa et al. proposed a method based on incremental modifications of the substrate holder by adding a ring to enlarge the size of the BEN area. This method is promising and has led to the formation of a film on almost the entire 2-inch substrate.[155]

The results obtained over the last few years are very significant and have made it possible to obtain films on much larger surfaces. Using a MgO substrate with the micro-needle concept, Aida et al. have obtained freestanding heteroepitaxial diamond film of 10x10mm^2 which exhibits a 0.07° FWHM of the diamond (004) reflection[144]. Lee et al. have used a scalable $SrTiO_3$/Si(100) substrate and produce a 7x7 mm^2 homogeneous heteroepitaxial film.[156] A silicon based heteroepitaxially grown diamond substrate of 10 mm in diameter has been produced to fabricate Schottky diodes; the FWHM of the substrate rocking curve is around 0.17° (600 arcsec)[148]. A freestanding heteroepitaxial diamond crystal with almost a circular shape with a dimension of 92 mm in pseudo-diameter has been obtained by Schreck et al. from Ir/YSZ/Si(100) with a FWHM of 0.064°+- 0.011° ((004) diamond reflection) and a high uniformity over two directions of the wafer (**Figure 6**).[129]

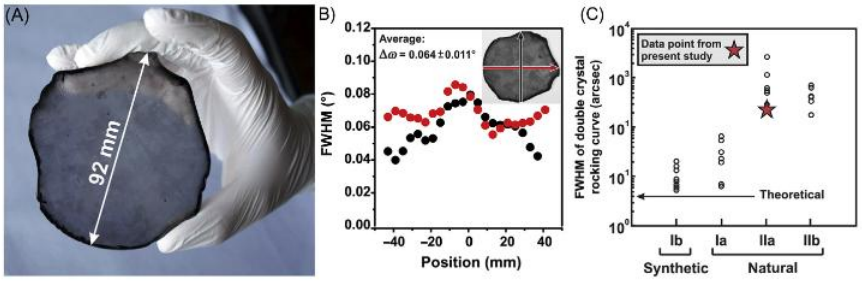

Figure 6. (A) Freestanding unpolished diamond single crystal synthesized by heteroepitaxy on Ir/YSZ/Si(0 0 1). The thickness of the disc is 1.6 ± 0.25 mm and its weight is 155 carat[129]. (B) FWHM values of two series of rocking curves measured along two perpendicular lines across the wafer. The average FWHM is 0.064 ± 0.011°. For the corresponding azimuthal scans [Dia(3 1 1)] a value of 0.12 ± 0.04° was obtained [129]. (C) Average width of rocking curves [129] plotted in the graph redrawn from Ref. [157]. YSZ, yttria stabilized zirconia; FWHM, full widths at half maximum. More details are provided in the following reference. [112] Reproduced with permission. Copyright 2018, Elsevier.

This shows that the maturity of heteroepitaxial diamond material is progressing quickly, as shown by the creation in 2015 of the company Audiatec from Germany, which markets heteroepitaxial diamond substrates for various applications and Adamant Namiki Precision Jewel company from Japan, which produces freestanding heteroepitaxial diamond films and targets large area wafers.

2.2.7 Applications of heteroepitaxial films

Many applications require films of very high crystalline quality because the presence of structural defects leads to a degradation of certain properties and therefore a reduction in expected performances. Although the crystalline quality of heteroepitaxial films is still far behind the quality of single crystals obtained by homeoepitaxy, the maturity of the material and recent progress have made it possible to integrate this material to carry out the first proofs of concept in various application fields. The path is promising as studies are focused on improving the crystalline quality and also the substrate upscaling which makes this material very credible for developing future high performance devices.

Diamond is an ideal material to monochromatize neutrons. As the beam is slightly divergent, the compromise between intensity and resolution requires crystals with a mosaic spread between 0.2° to 0.8°. Heteroepitaxial diamond film is thus an excellent candidate for this application. Fischer et al. have studied in detail the spatial distribution of the mosaic structure of heteroepitaxial diamond films with a size of 15x15x1mm^3.[158] In 2014, a first prototype composed of 16 crystal stacks with a mosaic spread between 0.25° and 0.30° has been evaluated at Institut Laue-Langevin. The proof of concept is demonstrated and they identified a limiting factor related to the non-uniformity of the spatial mosaic distribution.[159]

Heteroepitaxial diamond films have also a strong potential for particle detection because they allow large detectors. Berdermann et al. have evaluated heteroepitaxial diamond for large-area particle detectors[2]. The thin heteroepitaxial films they characterized are approaching the performance of single crystal diamond but the charge collection efficiency (CCE) for electron is lower and worse for thick films.

Power electronics is a very promising field for heteroepitaxial diamond but difficult to achieve because the crystalline quality of the films must be high enough to exploit the remarkable transport properties of diamond. In 2014 and 2015, the first electronic devices from heteroepitaxial films were produced: Takeuchi et al. have fabricated and characterized p-i-n diodes [147] and Kawashima et al. have produced Schottky barrier diodes[148] with a high rectification ratio above 10^{12} at +/- 4V, an ideality factor of 1.2 and a breakdown field around 1 MV/cm. In 2018, Syamsul et al. have explored the potential of heteroepitaxial diamond for FET for high voltage applications.[160]

The realization of diamond-based photonic devices also requires high quality substrates on which heteroepitaxial films could be used with the advantage of large wafer sizes and the possibility of integrating thin films which are essential for photonic systems that confine light. The potential of heteroepitaxial films for quantum applications based on color centers like nitrogen vacancy (NV) or silicon vacancy (SiV) hosted in diamond is therefore significant. Indeed, this material presents a high crystalline quality and large sizes, at lower cost compared to homoepitaxial diamond and is suitable for future quantum devices as highlighted by Schröder et al. in their study on quantum nanophotonics in diamond [66]. In 2016, Arend et al. have demonstrated a bottom-up approach to fabricate heteroepitaxial nano-structure array containing single SiV center[151]. In 2018, Yaita et al. demonstrated preferentially aligned NV centers on heteroepitaxial (111) diamond film having a spin coherence time (T_2) of 6µs comparable with homoepitaxial (111) diamond films.[152] A coherence time (T_2) of 5µs has been reported on (100) heteroepitaxial film in 2019 by Nelz et al.[161]

3. Current investigations (last reports 2020-2021)

3.1 Homoepitaxy

3.1.1. Growth at enhanced pressures

While typical pressures for SCD growth regimes in microwave plasma are currently within 100–400 Torr, a transition to much high pressures promises enhanced growth rates. The plasma stability at higher pressures, up to 600 Torr in CH_4-H_2 gas mixtures was demonstrated by Bolshakov et al.[162]. A strong change of the plasma shape and volume (the latter shrinks by 10 times at fixed MW power) with pressure rise from 100 to 600 Torr was observed, leading to a very high absorbed MW power density of ≈1800 W/cm^3. The diamond growth rate was found to increase by an order of magnitude

with the pressure to achieve ~60 μm/h at 500 Torr even at relatively low (4%) CH_4 concentration. The result can be regarded as a step towards atmospheric pressure MPCVD reactors, which have enhanced deposition rates and a less leakage in the vacuum system due to a decrease in pressure difference inside and outside the reactor. On the other hand, because of strong compression of the plasma cloud the high-pressure regime probably is not suitable for growth on multiple substrates which is preferable for an economically viable process.

3.2.2. Growth of thick crystals

Non-stop growth of diamond crystals with thickness significantly larger than 1 mm is difficult to realize as the increased size of the crystal causes a change of local process parameters such as the film-on-seed temperature and even plasma configuration. The vertical temperature gradient on the crystal edge can be well in excess of 100°C[163]. In addition, a polycrystalline diamond forms around the top surface of the substrate that also affects the thermal balance of the crystal and may induce a stress in it. As a partial solution, "repetitive growth" is used with periodical growth stops and resumptions. As an example, single crystals with thickness of up to 10 mm (4.65 ct) were produced in this way by Mokuno et al.[164] A drawback of the approach is not only a complexity of the procedure but also formation of defects and enhanced impurity concentration on the interfaces between successive layers.[165, 166] Recently Yamada et al.[*167*] succeeded in non-stop synthesis of ~6 mm thick crystal combining two ideas: (i) the undesired polycrystalline diamond growth on edges was partially suppressed by introducing oxygen into the source gas mixture, and (ii) a movable stage was introduced to continuously control distance from the top-surface of the plasma and core discharge during the process. Measurement of birefringence (Δn mapping) confirmed absence of non-uniformity across the crystal's depth. The approach actually was demonstrated for nitrogen doped-diamond, but should work also for production of high purity crystals (without adding N_2 in gas). The largest CVD diamond ever produced, of 46.2-carat rough, has been created by Shanghai Zhengshi Technology Co in 2020.[168]

3.2 Heteroepitaxy

3.2.1 Last insights into nucleation

A new substrate was very recently reported for heteroepitaxial (111) diamond. Indeed, (111) oriented diamond crystallites were obtained by BEN with a direct-current discharge on Ru (0001) epitaxially grown onto c-sapphire in an antenna edge type MPCVD.[119] The measured epitaxial relationship is [111] diamond // [0001] Ru and [112] diamond // [1010] Ru. In the perspective of large diamond (111) wafer production, ruthenium is a cheaper substrate compared to iridium.

The adsorption and desorption mechanisms of carbon atoms taking place at the iridium (100) surface were recently investigated by density functional theory (DFT).[169] According to these simulations, without applied bias, carbon and iridium atoms can strongly interact to form covalent bonds according to charge density mapping. Such interaction may occur locally and lead to a metastable Ir-C solid solution. Moreover, DFT calculations show that carbon-iridium bonds exhibit a sp^3 configuration. BEN induces a shallow carbon implantation into the iridium lattice via a dissolution precipitation mechanism. Carbon atoms can be desorbed to the surface vicinity. Under the flux of carbon species, rearrangement of sp^3 *nucleus* may occur. According to simulations, a window of bias voltage seems to be more favorable to diamond nucleation. In comparison, calculations do not support such a dissolution precipitation mechanism on copper or nickel (100) substrates. This study well illustrates the unique behavior of iridium for diamond heteroepitaxy.

HRTEM observations demonstrate the presence of nanometric diamond crystals at the iridium surface after BEN **(Figure 7)**.[131] The STEM-electron energy loss (EELS) spectrum recorded at carbon K edge confirms the diamond signature (Figure 4c). Fast Fourier Transforms (insert Figure 4a, b) showed a perfect orientation of the nanocrystal along the <110> zone axis with the epitaxial relationship diamond (002) [220] // iridium (002) [220]. This HRTEM report shows for the first time that such diamond crystals can be stable under BEN conditions. An in plane tensile strain of +7% is measured, huge compared to the one that can be underwent by bulk diamond (< 1%). This value is in the same order of magnitude as local tensile strain measured in diamond needles.[170]

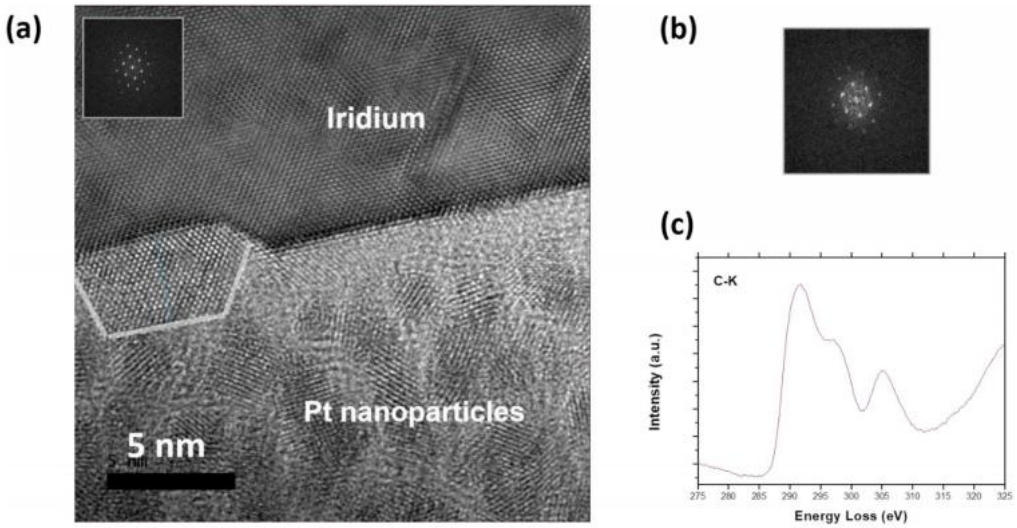

Figure 7. (a) HRTEM picture of an epitaxial diamond nanocrystal after BEN; (b) Fast Fourier Transform of the diamond nanocrystal; (c) C-K EELS spectrum recorded on such a nanocrystal. Reproduced with permission.[131] Copyright 2020, Elsevier.

A complete review of TEM investigations performed on different diamond materials appeared recently.[171] This paper particularly highlights benefits of TEM techniques in heteroepitaxy: from nucleation and interface characterization to studies of structural defects formation and dislocation propagation during growth.

Further progresses in heteroepitaxy, like improvement of the crystalline quality and the up-scaling control, may be possible by a deeper knowledge of nucleation kinetics. To monitor the *nuclei* formation and coalescence of *nuclei* at the early stages, *in situ* tools are required. Laser reflectometry, sensitive to the tridimensional growth mode, allowed a real time monitoring of nucleation on silicon.[172] Such an approach is hardly applicable to iridium due to the pseudo 2D structure of domains formed during BEN and the iridium surface roughening. The same conclusion can be drawn for the evolution of the bias current during BEN. It is also sensitive to the tridimensional mode observed on silicon or cubic silicon carbide and can be used for *in situ* nucleation monitoring on these substrates.[118] Delchevalrie et al showed recently the sensitivity of spectroscopic ellipsometry to domains formed during BEN on iridium.[173] Indeed, this technique probes optical index differences at interfaces. This contribution can be discriminated from the one related to the iridium surface roughening. These sequential *ex situ* characterizations pave the way to an *in situ* monitoring of diamond nucleation on iridium by spectroscopic ellipsometry.

3.2.2 Recent progress on dislocation reduction and structural quality improvement

The reduction of the dislocation density is still a challenge as it is certainly the most limiting factor for the development of applications integrating heteroepitaxial films. Efforts are continuing, recently Mehmel et al. have created in a heteroepitaxial film hole array of 500x500µm^2 by laser and studied the dislocation propagation bending according to lateral to normal growth rate which is the key parameter [174]. They obtained, in the closed hole, dislocation density as low as 6.10^5 cm^{-2}. Concerning the dislocation density, a non-destructive method of dislocations imaging for low boron doped diamond epilayer have been published recently[175] and could be potentially applied to heteroepitaxial diamond films.

The quality of heteroepitaxial films continues to improve, as evidenced in a recent study by Kim et al. where they synthesized a 1-inch free standing heteroepitaxial diamond wafer from sapphire (a-plane) with remarkable structural properties: FWHM of the X-ray rocking curve for diamond (004) is 113.4 arc sec (0.031°) which is one of the lowest values reported and a dislocation density of 1.4 10^7 cm^{-2}.[176] In the earlier reports, Ichikawa et al reported tilt and twist values of 0.064° and 0.043°,

respectively and a dislocation density of 9 10^6 cm^{-2}.[142] For Schreck et al., the minimum dislocation density was 7 10^6 cm^{-2} and tilt and twist values of 0.03° and 0.05°, respectively.[177]

Another challenge concerns the substrate size enlargement which is limited by the nucleation stage which remains difficult to apply in a controlled way on large surfaces and which is very dependent on the reactor considered. *In situ* diagnostic techniques have recently been published and may allow faster progress towards a more detailed understanding and control of the key mechanisms and key parameters involved in the BEN stage.[118, 173, 178]

3.2.3 Recent reports on impurities incorporation in heteroepitaxial diamond

Three other research groups reported on boron doping of heteroepitaxial diamond during the last year. First, a low boron doped overlayer (p-; 1.3 x10^{16} boron atoms per cm^3, 1.6 microns thick), was epitaxially grown onto a freestanding polished diamond grown by the same group on a Ir/$SrTiO_3$/Si (001) substrate. [131] The fabrication of lateral Schottky diodes over this substrate exhibits a high reproducibility for devices and the Schottky barrier height is in line with that measured for homoepitaxial diamond.

Two other groups started with a commercial freestanding heteroepitaxial diamond from Adamant Namiki Precision Jewel Co., Ltd. Electrical properties of several boron doped diamond epilayers were investigated. Hole concentrations were tuned from 1.1 x 10^{15} to 5 x 10^{19} per cm^3 at room temperature by increasing the boron concentration.[179] The doped epilayer with a boron concentration of 1 x 10^{18} atoms per cm^3 shows a mobility of 390 cm^2 V^{-1} s^{-1} according to Hall measurements. Such a value is intermediate compared to similar doped epilayer grown on homoepitaxial diamond **(Figure 8).**

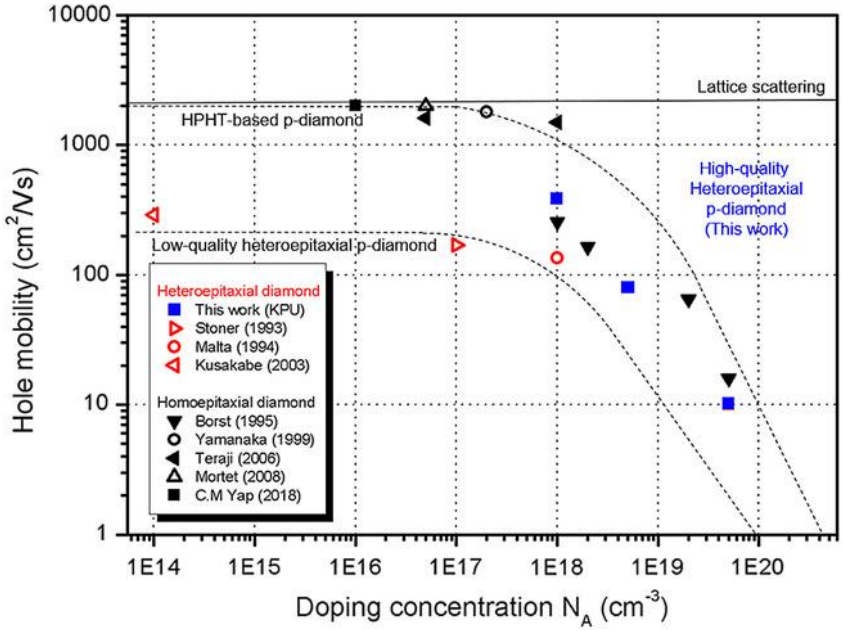

Figure 8. Hole mobility measured at 300 K versus the boron concentration for heteroepitaxial diamond compared to homoepitaxial diamond. Reproduced with permission.[179] Copyright 2020, Wiley-VCH GmbH.

More recently, to fabricate Schottky diodes, two boron doped p+ and p- overlayers, both 1 micron thick, were grown on this commercial heteroepitaxial diamond with boron concentrations of 1 x 10^{20} and 1 x10^{16} boron atoms per cm^3, respectively.[180] Diode performances were significantly affected by dislocations, with a reduced breakdown field. Further improvements of the heteroepitaxial material are necessary. A p+/p- structure was deposited by a second group on heteroepitaxial diamond from the same provider (Adamant Namiki Precision Jewel Co., Ltd). The highly boron doped layer (2.5 x 10^{20} boron atoms per cm^3) contains W impurities. Indeed, the presence of W atoms has a strong effect on the reduction of dislocation density (two orders of magnitude) during diamond growth of homoepitaxial diamond layers by hot filament CVD.[49] The behavior of these diodes is very close to

those measured for CVD or HPHT diamond substrates. This group measured the highest breakdown voltage ever reported for heteroepitaxial diamond (375 V).[181]

Concerning color center applications, single native NV centers were detected for the first time in heteroepitaxial diamond from Audiatec (Augsburg Diamond Technology GmbH) with a density of 1 NV per μm^3.[182] These NV centers are embedded in an ensemble of SiV centers. NV centers located close to the growth face exhibit the same performances (photoluminescence lifetime) than NV in diamond single crystals. A shallow nitrogen implantation and a further annealing permit generatation of NV centers within the 10 first nm. A surface nanostructuring allows fabrication of nanopillars containing NV centers. This study confirms the high potential of heteroepitaxial diamond for quantum devices on a large scale.

3.2.4 Recent trends in applications

Over the last few years, several heterosubstrates are being studied and developed in parallel with different layer building strategies to improve the crystalline quality of heteroepitaxial films. The maturity of the heteroepitaxial diamond has reached a stage where it is now possible to integrate it to fabricate the first devices and thus be able to measure and to benchmark their performances. A Schottky diode fabricated on sapphire base substrate was demonstrated by Kwak et al. with an ideality factor of 1.4 and a maximum breakdown field of 1.1 MV/cm [180]. J.C. Arnault et al. have successfully fabricated lateral Schottky diodes from Ir/$SrTiO_3$/Si(100) substrate and obtained I-V characteristics evidenced a yield of working diodes equal to 92% (on the same substrate of 7x7mm^2), close to that obtained for diodes on homoepitaxial films. To reduce the dislocation density, the metal impurity-incorporated buffer layer was integrated to fabricate pseudo-vertical Schottky diodes by Sittimart et al. [181]. The rectification ratio exceeds eight orders of magnitude and the breakdown field strength was 1.7 MV/cm. Murooka et al. have demonstrated and characterized Schottky diodes on heteroepitaxial films grown on 3C-SiC/Si substrates [183] and obtained a rectification ratio above 10^9 at +-5V. MOSFET have been recently developed by Saha et al [184] with a Baliga's Figure-Of-Merits of 145 MW/cm^2 and inversion channel MOSFET by Zhang et al. [185]. Recently, modulation-doped diamond FETs have been achieved using NO_2 delta doping in Al_2O_3 gate layer associated with a mobility of 2465 $cm^2.V^{-1}.s^{-1}$ near the threshold voltage [186].

These recent developments demonstrate the maturity reached by the heteroepitaxial diamond and its potential for the development of lower cost devices given the increasing size of the substrates. The presence of structural defects and dislocations in particular remains the most limiting element.

4. Conclusion and future trends

Homoepitaxial and heteroepitaxial diamond thin films, plates and crystals produced by MPCVD already possess properties acceptable for many applications, especially for realization of electronic and photonic devices and components. Further improvement of CVD diamond quality and size (and production cost) are of primary importance to further open the potential of this material for different applications and technologies. The homoepitaxial films surpass the heteroepitaxial ones in quality, the latter having advantage of much larger size, with diameter approaching to 4 inches, however suffering from high stress. Dislocation density in homoepitaxial diamond varies between 10^3 cm^{-2} to 10^7 cm^{-2}, while for the films on Ir substrate it is still higher, from to 10^7 cm^{-2} to 10^{10} cm^{-2}.[142] The latest reports look promising to further reduce dislocation density in the 10^5 cm^{-2} for heteroepitaxial diamond.[174] Note that HPHT diamond has a more perfect structure (dislocation density of 10^0 to 10^7 cm^{-2}) but contains more nitrogen impurities, and its size is limited.[10] Currently, because of specific features of the homoepitaxial and heteroepitaxial diamonds, they have own fields of applications, which, however, significantly cross each other.

Ultrapure low-strain homoepitaxial diamond films and plates of "quantum grade" are ideal to engineer various color centers with very narrow luminescence line even for large ensembles of the emitters. Radiation detectors require very high quality to obtain high mobility and long life-time of carriers, this is easier to realize on homoepitaxial films and plates. The detectors of different sorts, including multipixel sensors, were built on homoepitaxial samples, all on a single piece of diamond only, not on

large size mosaics. Position sensitive detectors needed for monitoring large aperture radiation fluxes require at least inch-scale electronic grade diamond wafers, either mosaics crystals or heteroepitaxial plates. Recent measurements of Diamond-on-Iridium (DOI) sensors on synchrotrons reveal that, in many aspects, the performance of those devices was quite similar to that of homoepitaxial counters, and in any case far superior to that of long time developed polycrystalline detectors[2] and may approach to properties of homoepitaxial films.

In the case of homoepitaxy the problem of crystal enlargement was most often focused on the lateral size increase, particularly by side growth. Now, with construction of substrate holders capable of Z-moving to keep the crystal-plasma distance constant, a way opened to produce very thick (more than 10 mm) diamond crystals. It is not excluded that in future it will be the vertical dimension which would determine the largest size of such crystals, and the crystal will approach 1 inch scale, at least vertically. Only homoepitaxial crystals were used so far for making diamond Raman lasers because of their low dislocation density coupled to large enough size and purity. The DRL reached 1 kW level, and a perspective to further increase the output power could be related to use of isotopically modified crystals (with isotope ^{12}C content better than 99.9%) which have enhanced thermal conductivity.

In the field of electronic devices, ~~the activity on~~ use of homoepitaxial films is far more advanced compared to heteroepitaxial diamond. The reasons are the long years of experimental work with the former, and continuing better quality. While both *p*-type and *n*-type doping were developed for homoepitaxial films, practically only boron doping was studied till now for heteroepitaxial films, and Schottky diodes were fabricated on B-doped diamond. P-i-n structures require also doping with phosphorus which was reported for heteroepitaxial films only in one study. The interest in n-doping is likelyt to grow rapidly in view of recent improvement in quality of heteroepitaxial diamond. There is a hope that with a further progress in understanding of growth process (including substrate pretreatment) and deposition technology, the gap in properties between the material produced by two the methods of epitaxy will narrow in the future.

References

[1] N. Donato, N. Rouger, J. Pernot, G. Longobardi, F. Udrea, *J. Phys. D: Appl. Phys.* **2020**, *53*, 093001.

[2] E. Berdermann, K. Afanaciev, M. Ciobanua, M. Fischer, S. Gsell, M. Kiš, S. Lagomarsino, W. Lohmann, M. Mayr, M. Pomorski, M.S. Rahmana, C.J. Schmidt, S. Sciortino, M. Schreck, C. Stehl, M. Träger, *Diam. Relat. Mater.* **2019**, *97*, 107420.

[3] K. Liu, S. Zhang, V. Ralchenko, P. Qiao, J. Zhao, G. Shu, L. Yang, J. Han, B. Dai, J. Zhu, *Adv. Mater.* **2021**, *33*, 2000891.

[4] C. Bradac, W. Gao, J. Forneris, M. E. Trusheim, I. Aharonovich, *Nature Comm.* **2019**, *10*, 5625.

[5] S. Pezzagna, J. Meijer, *Appl. Phys. Rev.* **2021**, *8*, 011308.

[6] S. Hong, M. S. Grinolds, L. M. Pham, D. Le Sage, L. Luan, R. L. Walsworth, A. Yacoby, *MRS Bulletin* **2013**, *38*, 155.

[7] S. Sotoma, C. P. Epperla, H. C. Chang, *ChemNanoMat* **2018**, *2*, 15.

[8] A. Ajoy, R. Nazaryan, E. Druga, K. Liu, A. Aguilar, B. Han, M. Gierth, J. T. Oon, B. Safvati, R. Tsang, J. H. Walton, D. Suter, C. A. Meriles, J. A. Reimer, A. Pines, *Rev. Sci. Instrum.* **2020**, *91*, 023106.

[9] J Achard, V. Jacques, A. Tallaire, *J. Phys. D: Appl. Phys.* **2020**, *53*, 313001.

[10] E. A. Ekimov, M. V. Kondrin, *Physics Uspekhi* **2017**, *60*, 539.

[11] J. M. Smith, S. A. Meynell, A. C. Bleszynski Jayich, J. Meijer, *Nanophotonics* **2019**, *8*, 1889.

[12] M. Schreck, J. Asmussen, S. Shikata, J. C. Arnault, N. Fujimori, *MRS Bulletin* **2014**, *39*, 504.

[13] M. Kasu, *Progress in Crystal Growth and Characterization of Materials* **2016**, *62*, 317.

[14] M. Schwander, K. Partes, *Diam. Relat. Mater.* **2011**, *20*, 1287.

[15] Y. N. Palyanov, I. N. Kupriyanov, A. F. Khokhryakov, V. G. Ralchenko, *Crystal Growth of Diamond*. In *Handbook of Crystal Growth*, 2015, pp. 671-713, Elsevier.

[16] J. Isberg, J. Hammersberg, E. Johansson, T. Wikstrom, D. J. Twitchen, A. J. Whitehead, S. E. Coe, G. A. Scarsbrook, *Science* **2002**, *297*, 1670.

[17] A. V. Inyushkin, A. N. Taldenkov, V. G. Ralchenko, A. P. Bolshakov, A. V. Koliadin, A. N. Katrusha, *Phys. Rev. B* **2018**, *97*, 144305.

[18] C. J. Widmann, M. Hetzl, S. Drieschner, C. E. Nebel, *Diam. Relat. Mater.* **2017**, *72*, 41.

[19] A. Tallaire, J. Achard, A. Boussadi, O. Brinza, A. Gicquel, I. N. Kupriyanov, Y. N. Palyanov, G. Sakr, J. Barjon, *Diam. Relat. Mater.* **2014**, *41*, 34.

[20] M. Lesik, T. Plays, A. Tallaire, J. Achard, O. Brinza, L. William, M. Chipaux, L. Torraile, T. Debuisschert, A. Giquel, J. F. Roch, V. Jacques, *Diam. Relat. Mater.* **2015**, *56*, 47.

[21] M. A. Pinault-Thaury, S. Temgoua, R. Gillet, H. Bensalah, I. Stenger, F. Jomard, R. Issaoui, J. Barjon, *Appl. Phys. Lett.* **2019**, *114*, 112106.

[22] M. Naamoun, A. Tallaire, F. Silva, J. Achard, P. Doppelt, A. Gicquel, *Phys. Status Solidi A* **2012**, *209*, 1715.

[23] V. Yurov, E. Bushuev, A. Bolshakov, E. Ashkinazi, I. Antonova, E. Zavedeev, A. Khomich, V. Voronov, V. Ralchenko, *Phys. Status Solidi A* **2017**, 1700177.

[24] A. Tallaire, J. Achard, F. Silva, R. S. Sussmann, A. Gicquel, E. Rzepka, *Phys. Status Solidi A* **2004**, *201*, 2419.

[25] J. Achard, A. Tallaire, V. Mille, M. Naamoun, O. Brinza, A. Boussadi, L. William, A. Gicquel, *Phys. Status Solidi A*, **2014**, *211*, 2264.

[26] I. Friel, S. L. Clewes, H. K. Dhillon, N. Perkins, D. J. Twitchen, G. A. Scarsbrook, *Diam. Relat. Mater*. **2009**, *18*, 808.

[27] A. B. Muchnikov, A. L. Vikharev, J. E. Butler, V. V. Chernov, V. A. Isaev, S. A. Bogdanov, A. I. Okhapkin, P. A. Yunin, Y. N. Drozdov, *Phys. Status Solidi A* **2015**, *212*, 2572

[28] M. L. Hicks, A. C. Pakpour-Tabrizi, V. Zuerbig, L. Kirste, C. Nebel, R. B. Jackman, *J. Appl. Phys*, **2019**, *125*, 244502.

[29] J. Lu, Y. Gu, T.A. Grotjohn, T. Schuelke, J. Asmussen, *Diam. Relat. Mater*. **2013**, *37*, 17.

[30] M. Muehle, J. Asmussen, M. F. Becker, T. Schuelke, *Diam. Relat. Mater*. **2017**, *79*, 150.

[31] J. Achard, A. Tallaire, R. Sussmann, F. Silva, A. Gicquel, *J. Cryst. Growth* **2005**, *284*, 396.

[32] E. V. Bushuev, V. Yu. Yurov, A. P. Bolshakov, V. G. Ralchenko, A. A. Khomich, I. A. Antonova, E. E. Ashkinazi, V. A. Shershulin, V. P. Pashinin, V. I. Konov, *Diam. Relat. Mater*. **2017**, *72*, 61]

[33] A. Chayahara, Y. Mokuno, Y. Horino, Y. Takasu, H. Kato, H. Yoshikawa, N. Fujimori, *Diam. Relat. Mater*. **2004**, *13*, 1954.

[34] A. B. Muchnikov, A. L. Vikharev, A. M. Gorbachev, D. B. Radishev, V. D. Blank, S. A. Terentiev, *Diam. Relat. Mater*. **2010**, *19*, 432.

[35] Q. Liang, C.Y. Chin, J. Lai, C.S. Yan, Y. Meng, H.K. Mao, R.J. Hemley, *Appl. Phys. Lett*. **2009**, *94*, 024103.

[36] E. V. Bushuev, V. Yu. Yurov, A. P. Bolshakov, V. G. Ralchenko, E. E. Ashkinazi, A. V. Ryabova, I. A. Antonova, P. V. Volkov, A. V. Goryunov, A. Yu. Luk'yanov, *Diam. Relat. Mater*. **2016**, *66*, 83.

[37] J. Asmussen, T. A. Grotjohn, T. Schuelke, M. F. Becker, M. K. Yaran, D. J. King, S. Wicklein, D. K. Reinhard, *Appl. Phys. Lett*. **2008**, *93*, 031502

[38] Q. Liang, C. S. Yan, J. Lai, Y. F. Meng, S. Krasnicki, H. Shu, H.-K. Mao, R. J. Hemley, *Cryst. Growth Design*, **2014**, *14*, 3234.

[39] A. De Sio, M. Di Fraia, M. Antonelli, R.H. Menk, G. Cautero, S. Carrato, L. Tozzetti, J. Achard, A. Tallaire, R.S. Sussmann, E. Pace, *Diam. Relat. Mater*. **2013**, *34*, 36.

[40] S. Nad, A. Charris, J. Asmussen, *Appl. Phys. Lett*. **2016**, *109*, 162103.

[41] Y. Mokuno, A. Chayahara, H. Yamada, N. Tsubouchi, *Diam. Relat. Mater*. **2009**, *18*, 1258.

[42] M. W. Geis, H. I. Smith, A. Argoitia, J. Angus, G.-H. M. Ma, J. T. Glass, J. Butler, C. J. Robinson, R. Pryor, *Appl. Phys. Lett*. **1991**, *58*, 2485.

[43] G. Janssen, L. J. Giling, *Diam. Relat. Mater*. **1995**, *4*, 1025.

[44] H. Yamada, A. Chayahara, Y. Mokuno, N. Tsubouchi, S. Shikata, *Diam. Relat. Mater*. **2013**, *33*, 27.

[45] H. Yamada, A. Chayahara, Y. Mokuno, Y. Kato, S. Shikata, *Appl. Phys. Lett*. **2014**, *104*, 102110

[46] H. Yamada, A. Meier, F. Mazzocchi, S. Schreck, T. Scherer, *Diam. Relat. Mater*. **2015**, *58*, 1.

[47] S. Bogdanov, A. Vikharev, A. Gorbachev, A. Muchnikov, D. Radishev, N. Ovechkin, V. Parshin, *Chem. Vapor Depos.* **2014**, *20*, 32.

[48] G. Shu, B. Dai, V. G. Ralchenko, A. A. Khomich, E. E. Ashkinazi, A. P. Bolshakov, S. N. Bokova-Sirosh, K. Liu, J. Zhao, J. Han, J. Zhu, *J. Cryst. Growth* **2017**, *463*, 19.

[49] S. Ohmagari, H. Yamada, N. Tsubouchi, H. Umezawa, A. Chayahara, A. Seki, F. Kawaii, H. Saitoh, Y. Mokuno, *Appl. Phys. Lett*. **2019**, *114*, 082104.

[50] S. Ohmagari, H. Yamada, N. Tsubouchi, H. Umezawa, A. Chayahara, Y. Mokuno, D. Takeuchi, *Phys. Status Solidi A*, **2019**, *216*, 1900498.

[51] H. Umezawa, Mater. Sci. Semicond. Proc. **2018**, *78*, 147.

[52] M. W. Geis, T. C. Wade, C. H. Wuorio, T. H. Fedynyshyn, B. Duncan, M. E. Plaut, J. O. Varghese, S. M. Warnock, S. A. Vitale, M.A. Hollis, *Phys. Status Solidi A*, **2018**, *215*, 1800681.

[53] A. Tallaire, A. Valentin, V. Mille, L. William, M. A. Pinault-Thaury, F. Jomard, J. Barjon, J. Achard, *Diam. Relat. Mater.* **2016**, *66*, 61.

[54] H. Kato, M. Ogura, T. Makino, D. Takeuchi, S. Yamasaki, *Appl. Phys. Lett*. **2016**, *109*, 142102.

[55] G. Chicot, A. Fiori, P. Volpe, T.T. Thi, J. Gerbedoen, J. Bousquet, *J. Appl. Phys*. **2014**, 116, 083702.

[56] J. E. Butler, A. Vikharev, A. Gorbachev, M. Lobaev, A. Muchnikov, D. Radischev, V. Isaev, V. Chernov, S. Bogdanov, M. Drozdov, E. Demidov, E. Surovegina, V. Shashkin, A. Davydov, H. Tan, L. Meshi, A.C. Pakpour-Tabrizi, M.L. Hicks, R. B. Jackman, *Phys. Status Solidi – RRL*, **2017**, *11*, 1600329.

[57] M. A. Lobaev, A. M. Gorbachev, A. L. Vikharev, V. A. Isaev, D. B. Radishev, S. A. Bogdanov, M. N. Drozdov, P.A. Yunin, J. E. Butler, *Thin Solid Films*, **2018**, *653*, 215.

[58] M. A. Lobaev, A. M. Gorbachev, S. A. Bogdanov, A. L. Vikharev, D. B. Radishev, V. A. Isaev, M. N. Drozdov, *Phys. Status Solidi A* **2018**, *215*, 1800205.

[59] S. A. Bogdanov, S. V. Bolshedvorskii, A. I. Zeleneev, V. V. Soshenko, O. R. Rubinas, D. B. Radishev, M. A. Lobaev, A. L. Vikharev, A. M. Gorbachev, M. N. Drozdov, A.V. Akimov, *Mater. Today Comm.* **2020**, *24*, 101019].

[60] K. G. Crawford, I. Maini, D. A. Macdonald, D. A. Moran, *Progr. Surf. Sci.* **2021**, *96*, 100613.

[61] H. Kawarada, *Jpn. J. Appl. Phys.* **2012**, 51, 090111.

[62] G. Conte, E. Giovine, A. Bolshakov, V. Ralchenko, V. Konov, *Nanotechnology* **2012**, *23*, 025201.

[63] C. Verona, M. Benetti, D. Cannat`a, W. Ciccognani, S. Colangeli, F.D. Pietrantonio, E. Limiti, M. Marinelli, G. Verona-Rinati, *IEEE Electron Device Lett*. **2019**, *40*, 765.

[64] M. Kasu, *Jpn. J. Appl. Phys. Part 1*, **2017**, *56*, 01AA01.

[65] S.A.O. Russell, S. Sharabi, A. Tallaire, D.A.J. Moran, *IEEE Electron Dev. Lett*. **2012**, 33 1471.

[66] T. Schröder, S.L. Mouradian, J. Zheng, M.E. Trusheim, M. Walsh, E.H. Chen, L. Li, I. Bayn, D. Englund, *JOSA B* **2016**, *33*, B65.

[67] R. E. Evans, A. Sipahigil, D. D. Sukachev, A. S. Zibrov, M. D. Lukin, *Phys. Rev. Appl.* **2016**, *5*, 044010.

[68] V. G. Ralchenko, V. S. Sedov, A. K. Martyanov, A. P. Bolshakov, K. N. Boldyrev, V. S. Krivobok, S. N. Nikolaev, S. V. Bolshedvorskii, O. R. Rubinas, A. V. Akimov, A. A. Khomich, E. V. Bushuev, R. A. Khmelnitsky, V. I. Konov, *ACS Photonics* **2019**, *6*, 66.

[69] V. Sedov, A. Martyanov, S. Savin, A. Bolshakov, E. Bushuev, A. Khomich, O. Kudryavtsev, V. Krivobok, S. Nikolaev, V. Ralchenko, *Diam. Relat. Mater.* **2018**, *90*, 47.

[70] G. Balasubramanian, P. Neumann, D. Twitchen, M. Markham, R. Kolesov, N.Mizuochi, J. Isoya, J. Achard, J. Beck, J. Tissler, V. Jacques, P. R. Hemmer, F. Jelezko, J. Wrachtrup, *Nat. Mater.* **2009**, *8*, 383.

[71] T. Teraji, T. Yamamoto, K. Watanabe, Y. Koide, J. Isoya, S. Onoda, T. Ohshima, L. J. Rogers, F. Jelezko, P. Neumann, J. Wrachtrup, S. Koizumi, *Phys. Status Solidi A* **2015**, *212*, 2365.

[72] Y. Mokuno, A. Chayahara, H. Yamada, N. Tsubouchi, *Diam. Relat. Mater.* **2010**, *19*, 128.

[73] K. Desjardins, C. Menneglier, M. Pomorski, *J. Instrumentation*, **2017**, *12*, C12046.

[74] S. Stoupin, T. Krawczyk, Z. Liu, C. Franck, *Crystals*, **2019**, *9*, 396.

[75] N. Kujala, M. Makita, J. Liu, A. Zozulya, M. Sprung, C. David, J. Grünert, *J. Synchrotron Rad.* **2019**, *26*, 708.

[76] R. S. Balmer, J. R. Brandon, S. L. Clewes, H. K. Dhillon, J. M. Dodson, I. Friel, P. N. Inglis, T. D. Madgwick, M. L. Markham, T. P. Mollart, N. Perkins, G. A. Scarsbrook, D. J. Twitchen, A. J. Whitehead, J. J. Wilman, S. M. Woollard, *J. Phys.: Condens. Matter* **2009**, *21*, 364221.

[77] P. Barberet, M. Pomorski, G. Muggiolu, E. Torfeh, G. Claverie, C. Huss, S. Saada, G. Deves, M. Simon, H. Seznec, *Appl. Phys. Lett.* **2017**, *111*, 243701.

[78] M. Angelone, G. Aielli, S. Almaviva, R. Cardarelli, D. Lattanzi, M. Marinelli, E. Milani, G. Prestopino, M. Pillon, R. Santonico, A. Tucciarone, C. Verona, G. Verona-Rinati, *IEEE Trans. Nucl. Sci*. **2009**, *56*, 2275.

[79] C. Y. Lee, C. M. Ban, H. R. Lee, K. N. Choo, B. H. Jun, *Appl. Rad. Isotopes* **2019**, *152*, 25.

[80] A.P. Bolshakov, K.N. Zyablyuk, V.A. Kolyubin, V.A. Dravin, R.A. Khmelnitskii, P.G. Nedosekin, V.N. Pashentsev, E.M. Tyurin, V.G. Ralchenko, *Nuclear Instrum. Methods A,* **2017**, *871*, 142.

[81] K. Liu, B. Dai, V. Ralchenko, Y. Xia, B. Quan, J. Zhao, G. Shu, G. Gao, L. Yang, P. Lei, J. Han, J. Zhu, *Sensors and Actuators A* **2017**, *259*, 121.

[82] F. Marsolat, D. Tromson, N. Tranchant, M. Pomorski, C. Bassinet, C. Huet, S. Derreumaux, M. Chea, K. Cristina, G. Boisserie, I. Buchheit, V. Marchesi, S. Gaudaire-Josset, A. Lisbona, D. Lazaro, R. Hugon, P. Bergonzo, *J. Appl. Phys.* **2015**, *118*, 234507.

[83] A. Oh, B. Caylar, M. Pomorski, T. Wengler, *Diam. Relat. Mater.* **2013**, *38*, 9.

[84] F. Bachmair, L. Bäni, P. Bergonzo, B. Caylar, G. Forcolin, I. Haughton, D. Hits, H. Kagan, R. Kass, L. Li, A. Oh, S. Phan, M. Pomorski, D. S. Smith, V. Tyzhnevyi, R. Wallny, D. Whitehead, *Nuclear Instrum. Methods A* **2015**, *786*, 97.

[85] S. Lagomarsino, M. Bellini, C. Corsi, F. Gorelli, G. Parrini, M. Santoro, S. Sciortino, *Appl. Phys. Lett*. **2013**, *103*, 233507.

[86] T. Kononenko, V. Ralchenko, A. Bolshakov, V. Konov, P. Allegrini, M. Pacilli, G. Conte, E. Spiriti, *Appl. Phys. A* **2014**, *114*, 297.

[87] C. Bloomer, M. E. Newton, G. Rehm, P. S. Salter, *J. Synchrotron Rad*. **2020**, *27*, 599.

[88] A. A. Khomich, K. K. Ashikkaliev, A. P. Bolshakov, T. V. Kononenko, V. G. Ralchenko, V. I. Konov, P. Oliva, G. Conte, S. Salvatori, *Diam. Relat. Mater.* **2018**, *90*, 84.

[89] T.V. Kononenko, A.A. Khomich, V.I. Konov, *Diam. Relat. Mater*. **2013**, *37* 50.

[90] S. Lagomarsino, M. Bellini, C. Corsi, S. Fanetti, F. Gorelli, I. Liontos, G. Parrini, M. Santoro, S. Sciortino, *Diam. Relat. Mater.* **2014**, *43*, 23.

[91] S. Salvatori, M. C. Rossi, G. Conte, T. V. Kononenko, M. S. Komlenok, A. A. Khomich, V. G. Ralchenko, V. I. Konov, G. Provatas, M. Jaksic, *IEEE Sensors Journal*, **2019**, *19*, 11908.

[92] K. K. Ashikkalieva, T. V. Kononenko, E. A. Obraztsova, E. V. Zavedeev, E. E. Ashkinazi, A. A. Mikhutkin, A.A. Khomivh, V.I. Konov, *Diam. Relat. Mater*. **2019**, *91*, 183.

[93] P. Oliva, S. Salvatori, G. Conte, A. P. Bolshakov, V. G. Ralchenko, Diamond detectors with graphite contacts. *Chapter 2,* in *Advances in Sensors Review*, ed. by S. Y. Yurish, (2018), IFSA Publishing, SL.

[94] R. P. Mildren, A. Sabella, O. Kitzler, D. J. Spence, A. M. Mckay, Diamond Raman laser design and performance, in *Optical Engineering of Diamond*. Weinheim, Germany: Wiley-VCH Verlag GmbH, 2013, pp. 239–276.

[95] R. J. Williams, O. Kitzler, Z. Bai, S. Sarang, H. Jasbeer, A. McKay, S. Antipov, A. Sabella, O. Lux, D. J. Spence, R. P. Mildren, *IEEE J. Select. Topics. Quantum Electron*. **2018**, *24*, 1602214.

[96] G. Eckhardt, D. Bortfeld, M. Geller, *Appl. Phys. Lett.* **1963**, *3*, 137.

[97] A.A. Kaminskii, V.G. Ralchenko, V.I. Konov, *JETP Lett.* **2004**, *80*, 267.

[98] A. A. Kaminskii, R. J. Hemley, J. Lai, C. S. Yan, H. K. Mao, V. G. Ralchenko, H. J. Eichler, H. Rhee, *Laser Phys. Lett.* **2007**, *4*, 350.

[99] R. P. Mildren, J. E. Butler, J. R. Rabeau, *Opt. Express*, **2008**, *16*, 18950.

[100] S. Antipov, A. Sabella, R. J. Williams, O. Kitzler, D. J. Spence, R. P. Mildren, *Opt. Lett.* **2019**, *44*, 2506.

[101] M. Murtagh, J. Lin, R. P. Mildren, G. McConnell, D. J. Spence, *Opt. Express*, **2015**, *23*, 15504; A. Sabella, J. A. Piper, R. P. Mildren, *Opt. Lett.* **2014**, *39*, 4037.

[102] C. L. Jia, K. Urban, X. Jiang, *Phys. Rev. B* **1995**, *52*, 5164.

[103] X. Jiang and C.-P. Klages, *Phys. Status Solidi A* **1996**, *154*, 175.

[104] S. D. Wolter, M. T. McClure, J. T. Glass, B. R. Stoner, *Appl. Phys. Lett.* **1995**, *66*, 2810.

[105] W. Liu, D. A. Tucker, P. Yang, J. T. Glass, *J. Appl. Phys.* **1995**, *78*, 1291.

[106] T. Tachibana, Y. Yokota, K. Nishimura, K. Miyata, K. Kobashi, Y. Shintani, *Diam. Relat. Mater.* **1996**, *5*, 197.

[107] K. Ohtsuka, K. Suzuki, A. Sawabe, T. Inuzuka, *Japanese Journal of Applied Physics Part 2-Letters*, **1996**, *35*, L1072-L1074.

[108] H. Maeda, S. Masuda, K. Kusakabe, S. Morooka, *Diam. Relat. Mater.* **1994**, *3*, 398.

[109] M. Yoshimoto, K. Yoshida, H. Maruta, Y. Hishitani, H. Koinuma, S. Nishio, *Nature*, **1999,** *399*, 340.

[110] W. Zhu, P. C. Yang, J. T. Glass, *Appl. Phys. Lett.* **1993**, *63*, 1640.

[111] T. Bauer, M. Schreck, S. Gsell, F. Hörmann, B. Stritzker B, *Phys. Status Solidi A* **2003,** *199*, 19.

[112] M. Schreck and J. C. Arnault, in Power Electronics Device Applications of Diamond Semiconductors (Eds S. Koizumi, H. Umezawa, J. Pernot, M. Suzuki), Elsevier, Duxford, **2018**, Ch.1.4

[113] T. Fujisaki, M. Tchiki, N. Taniyama, M. Kudo, H. Kawarada, *Diam. Relat. Mater.* **2002**, *11*, 478.

[114] S. Kim, Y Kawamata, R Takaya, K. Koyama, M Kasu, *Appl. Phys. Lett.* **2020**, 117, 202102

[115] Q. Wang, G Wu, T. A. Newhourse-Illige , A. W. Shepard, J. A. Greer, Z. Gan, G. Feng , S. Liu, *Diam. Relat. Mater.* **2020**, *110*, 108117.

[116] L. Fan, C. B. Jacobs, C. M. Rouleau, G. Eres, *Cryst. Growth Des.* **2017**, 17, 89−94.

[117] M. Frank, O.Sabine, G. Andreas, R. Eduard, C. Regine, F. Alexander, W. Marco, G. Lukas, B. Frank, *Thin Solid Films* **2018**, Vol. 650, 65-70.

[118] J. Yaita, T. Suto, M. R. Natal, S. E. Saddow, M. Hatano, T. Iwasaki, *Diam. Relat. Mater.* **2018**, *88, 158*

[119] W. Fei, K. Wei, A. Morishita, H. Wang, H. Kawarada, *Appl. Phys. Lett*. **2020,** *117*, 112102.

[120] J.C. Arnault, *Surf. Rev and Letters* **2003**, *10*, 127.

[121] S. Yugo, T. Kanai , T. Kimura, T. Muto, *Appl. Phys. Lett.* **1991**, *58*, 1036.

[122] K. Ohtsuka, K. Suzuki, A. Sawabe, T. Inuzuka, *Jpn J. Appl. Phys.* **1996**, *35*, L1072.

[123] A. Chavanne, J. C. Arnault, J. Barjon, J. Arabski, *Surf. Sci.* **2011**, *605*, 564.

[124] J. Yaita, M. Natal, S. E. Saddow, M. Hatano, T. Iwasaki, *Appl. Phys. Express* **2017**, *10*, 045502.

[125] J.C. Arnault, S. Saada, S. Delclos, L. Rocha, L. Intiso, R. Polini, A. Hoffman, S. Michaelson, P. Bergonzo, *Chem. Vap. Deposition* **2008**, *14*, 187.

[126] R. Brescia, M. Schreck, S. Gsell, M. Fischer, B. Stritzker, *Diam. Relat. Mater.* **2008**, *17*, 1045.

[127] S. Kono, T. Takano, T. Goto, Y. Ikejima, M. Shiraishi, T. Abukawa, T. Yamada, A. Sawabe, *Diam. Relat. Mater.* **2004**, *13*, 2081.

[128] N. Vaissière, S. Saada, M. Bouttemy, A. Etcheberry, P. Bergonzo, J.C. Arnault, *Diam. Relat. Mater.* **2013**, *36*, 16.

[129] M. Schreck, S. Gsell, R. Brescia, M. Fischer, *Scientific Report*, **2017**, *7*, 44462

[130] M. Schreck, A. Schury, F. Hörmann, H. Roll, B. Stritzker, *J. Appl. Phys.* **2002**, *91*, 676.

[131] J. C. Arnault, K.H. Lee, J. Delchevalrie, J. Penuelas, L. Mehmel, O. Brinza, S. Temgoua, I. Stenger, J. Letellier, G. Saint-Girons, R. Bachelet, R. Issaoui, A. Tallaire, J. Achard, J. Barjon, D. Eon, C. Ricolleau, S. Saada, *Diam. Relat. Mater.* **2020**, *105*, 107768.

[132] O. Klein, M. Mayr, M. Fischer, S. Gsell, M. Schreck, *Diam. Relat. Mater.* **2016**, *65*, 53.

[133] H. Bensalah, I. Stenger, G. Sakr, J. Barjon, R. Bachelet, A. Tallaire, J. Achard, N. Vaissiere, K.H. Lee, S. Saada, J.C. Arnault, *Diam. Relat. Mater.* **2016**, *66*, 188.

[134] M. Schreck, M. Mayr, O. Klein, M. Fischer, S. Gsell, A. F. Sartori, B. C. Gallheber, *Phys. Status Solidi A* **2016**, *213*, 2028.

[135] C. Stehl, M. Fischer, S. Gsell, E. Berdermann, M. S. Rahman, M. Traeger, O. Klein, M. Schreck, *Appl. Phys. Lett.* **2013**, *103*, 151905.

[136] M. Mayr, M. Fischer, O. Klein, S. Gsell, M. Schreck, *Phys. Status Solidi A* **2015**, *212*, 2480.

[137] B.C. Gallheber, O. Klein, M. Fischer, M. Schreck, *J. Appl. Phys.* **2017**, *121*, 225301.

[138] B.C. Gallheber, M. Fischer, M. Mayr, J. Straub, M. Schreck, *J. Appl. Phys.* **2018**, *123*, 225302. (111)

[139] Y. Ando, J. Kuwabara, K. Suzuki, A. Sawabe, *Diam. Relat. Mater.* **2004**, 13, 1975– 1979.

[140] K. Ichikawa, H. Kodama, K. Suzuki, A. Sawabea, *Diam. Relat. Mater.* **2017**, 72, 114-118.

[141] S. Washiyama, S. Mita, K. Suzuki, A. Sawabe, *Appl. Phys. Express* **2011**, 4 095502.

[142] K. Ichikawa, K. Kurone, H. Kodama, K. Suzuki, A. Sawabe, *Diamond Relat. Mater.* **2019**, 94, 92-100.

[143] Y. H. Tang, B. Golding, *Appl. Phys. Lett.* **2016**, 108, 052101.

[144] H. Aida, K. Ikejiri, S.W. Kim, K. Koyama, Y. Kawamata, H.Kodama, A. Sawabe, *Diam. Relat. Mater.* **2016**, 66, 77-82.

[145] H. Aida, S.W. Kim, K. Ikejiri, D. Fujii, Y. Kawamata, K. Koyama, H. Kodama, A. Sawabe, *Diam. Relat. Mater.* **2017**, 75, 34-38.

[146] H. Aida, S.W. Kim, K. Ikejiri, Y. Kawamata, K. Koyama, H. Kodama, A. Sawabe, *Applied Physics Express* **2016**, 9, 035504.

[147] D. Takeuchi, T. Makino, H. Kato, M. Ogura, N. Tokuda, T. Matsumoto, D. Kuwabara, H. Okushi, S. Yamasaki, *Phys. Status Solidi A* **2014**, *211*, 2251.

[148] H. Kawashima, H. Noguchi, T. Matsumoto, H. Kato, M. Ogura, T. Makino, S. Shirai, D. Takeuchi, S. Yamasaki, *Appl. Phys. Express* **2015**, *8*, 104103

[149] A. F. Sartori, M. Fischer, S. Gsell, M. Schreck, *Phys. Status Solidi A* **2012**, *209*, 1643.

[150] S. Turner, H. Idrissi, A. F. Sartori, S. Korneychuck, Y.-G. Lu, J. Verbeeck, M. Schreck, G. Van Tendeloo, *Nanoscale* **2016**, *8*, 2212.

[151] C. Arend, P. Appel, J. N. Becker, M. Schmidt, M. Fischer, S. Gsell, M. Schreck, C. Becher, P. Maletinsky, E. Neu, *Appl. Phys. Lett.* **2016**, *108*, 063111.

[152] J. Yaita, T. Tsuji, M. Hatano, T. Iwasaki, *Appl. Phys. Express* **2018**, *11*, 045501.

[153] G. Kucsko, P. C. Maurer, N. Y. Yao, M. Kubo, H. J. Noh, P. K. Lo, H. Park, M. D. Lukin, *Nature* **2013**, *500*, 54.

[154] M. Regmi, K. More, G. Eres, *Diam. Relat. Mater* **2012**, 23, 28.

[155] T. Yoshikawa, D. Herrling, F. Meyer, F. Burmeister, C. E. Nebel, O Ambacher, V. Lebedev, *J. Vac. Sci. Technol.* **2019**, B 37, 021207.

[156] K. H. Lee, S Saada, J.C. Arnault, R. Moalla, G. Saint-Girons, R. Bachelet, H. Bensalah, I. Stenger, J. Barjon, A. Tallaire, J. Achard, *Diam. Relat. Mater.* **2016**, *66*, 67.

[157] S. Fujii, Y. Nishibayashi, S. Shikata, A. Uedono, S. Tanigawa, *J. Appl. Phys.* **1995,** *78*, 1510.

[158] M. Fischer, A.K. Freund, S. Gsell, M. Schreck, P. Courtois, C. Stehl, G. Borchert, A. Ofner, M. Skoulatos, K.H. Andersen, *Diam. Relat. Mater.* **2013**, *37*, 41.

[159] P. Courtois, M. T. Fernandez-Diaz, G. Nenert, K. H. Andersen, A. K. Freund, S. Gsell, M. Fischer, M. Schreck, P. Link, M. Meven, *Journal of Physics: Conference Series* 528 **2014**, 012001.

[160] M. Syamsul , N. Oi, S. Okubo, T. Kageura, H. Kawarada, *IEEE Electron Device Letters* **2018**, *39*, 1.

[161] R. Nelz, J. Görlitz, D. Herrmann, A. Slablab, M. Challier, M. Radtke, M. Fischer, S. Gsell, M. Schreck, C. Becher, E. Neu, *APL Mater.* **2019**, *7*, 011108.

[162] A.P. Bolshakov, V.G. Ralchenko, G. Shu, B. Dai, V.Yu. Yurov, E.V. Bushuev, A.A. Khomich, A.S. Altakhov, E.E. Ashkinazi, I.A. Antonova, A.V. Vlasov, Y.Y. Sizov, S.K. Vartapetov, V.I. Konov, J. Zhu, *Mater.Today Comm*. **2020**, *25*, 101635.

[163] G. Shu, B. Dai, V.G. Ralchenko, A.P. Bolshakov, A.A. Khomich, E.E. Ashkinazi,V.Yu. Yurov, K. Yao, K. Liu, J. Zhao, J. Han, J. Zhu, *J. Cryst. Growth*, **2018**, *486*, 104

[164] Mokuno, Y., Chayahara, A., Soda, Y., Horino, Y., Fujimori, N. *Diam. Relat. Mater*. **2005**, *14*, 1743.

[165] Y. Mokuno, A. Chayahara, H. Yamada, N. Tsubouchi, *Diam. Relat. Mater*. **2010**, *19*, 128.

[166] G. Shu, V.G. Ralchenko, A.P. Bolshakov, E.V. Zavedeev, A.A. Khomich, P.A. Pivovarov, E.E. Ashkinazi, V.I. Konov, B. Dai, J. Han, J. Zhu, *CrystEngComm*, **2020**, *22*, 2138.

[167] H. Yamada, A. Chayahara, Y. Mokuno, *Diam. Relat. Mater*. **2020,** *101*, 107652.

[168] https://www.diamonds.net/news/NewsItem.aspx?ArticleID=65787.

[169] Y. Wang, W. Wang, G. Shu, S. Fang, B. Dai, J. Zhu, *J. Crystal Growth* **2021**, *560-561*, 126047.

[170] A. Banerjee, D. Bernoulli, H. Zhang, M.F. Yuen, J. Liu, J. Dong, F. Ding, J. Lu, M. Dao, W. Zhang, Y. Lu, S. Suresh, *Science* **2018**, *360*, 300.

[171] W. Jäger, in: *Semiconductors and semimetals* **2021**, *104*, 31.

[172] S. Saada, S. Pochet, L. Rocha, J.C. Arnault, P. Bergonzo, *Diam. Relat. Mater.* **2009**, *18*, 707.

[173] J. Delchevalrie, S. Saada, R. Bachelet, G. Saint-Girons, J. C. Arnault, *Diam. Relat. Mater.* **2021**, *112* 108246.

[174] L. Mehmel, R. Issaoui, O. Brinza, A. Tallaire, V. Mille, J. Delchevalrie, S. Saada, J. C. Arnault, F. Bénédic, J. Achard, *Appl. Phys. Lett.* **2021** *118*, 061901

[175] C. Barbay, S. Saada, C. Mer-Calfati, S. Temgoua, J. Barjon, J.C. Arnault, *Appl. Surf. Science* **2019** 495, 143564.

[176] S. Kim, Y Kawamata, R Takaya, K. Koyama, M Kasu, *Appl. Phys. Lett.* **2020**, 117, 202102

[177] M. Schreck, P. Ščajev, M. Träger, M. Mayr, T. Grünwald, M. Fischer, S. Gsell. Charge carrier trapping by dislocations in single crystal diamond. J. Appl. Phys. 2020, 127, 125102.

[178] H. Aida, R. Oshima, T. Ouchi, Y. Kimura, A. Sawabe, *Diam. Relat. Mater.* **2021**, 113, 108253.

[179] T. Kwak, J. Lee, G. Yoo, G. Yoo, H. Shin, U. Choi, B. So, S. Kim, O. Nam, *phys. stat. sol (a)* **2020**, *217*, 1900973.

[180] T. Kwak, J. Lee, U. Choi, B. So, G. Yoo, S. Kim, O. Nam, *Diam. Relat. Mater.* **2021**, *114* 108335.

[181] P. Sittimart, S. Ohmagari, T. Yoshitake, *Japanese Journal of Applied Physics* **2021**, *60*, SBBD05

[182] R. Nelz, J. Görlitz, D. Herrmann, A. Slablab, M. Challier, M. Radtke, M. Fischer, S. Gsell, M. Schreck, C. Becher, E. Neu, *APL Mater.* **2019**, *7*, 011108.

[183] T. Murooka, J. Yaita, T. Makino, M. Ogura, H. Kato, S. Yamasaki, M. Natal, S.E. Saddow, T. Iwasaki, M. Hatano, *IEEE Electron Device Lett.* **2020**, *67*, 212.

[184] N.C. Saha, T. Oishi, S.W. Kim, Y. Kawamata, K. Koyama, M. Kasu, *IEEE Electron Device Lett.* **2020**, *41*, 1066.

[185] X. Zhang, T. Matsumoto, Y. Nakano, H. Noguchi, H. Kato, T. Makino, D. Takeuchi, M. Ogura, S. Yamasaki, C. E. Nebel, T. Inokuma, N. Tokuda, *Carbon* **2021**, 175, 615-619.

[186] M. Kasu, N.C. Saha, T. Oishi, S.W. Kim, *Applied Physics Express* **2021**, 14, 051004.